Irrigation retrieval from Landsat optical/thermal data integrated into a crop water balance model: A case study over winter wheat fields in a semi-arid region

Luis Enrique Olivera-Guerra, Olivier Merlin, Salah Er-Raki

Irrigation retrieval from Landsat optical/thermal data integrated into a crop water balance model: A case study over winter wheat fields in a semi-arid region

Luis Olivera-Guerra[1*], Olivier Merlin[1], Salah Er-Raki[2,3]

** mail (olivera-guerrale@cesbio.cnes.fr)*

[1] Centre d'Etudes Spatiales de la Biosphère (CESBIO), Université de Toulouse, CNES, CNRS, IRD, UPS, Toulouse, France

[2] LP2M2E, Département de Physique Appliquée, Faculté des Sciences et Techniques, Université Cadi Ayyad, Marrakech, Morocco

[3]Center for Remote Sensing Application (CRSA), University Mohammed VI Polytechnic (UM6P), Benguerir, Morocco

ABSTRACT

Monitoring irrigation is essential for an efficient management of water resources in arid and semi-arid regions. We propose to estimate the timing and the amount of irrigation throughout the agricultural season using optical and thermal Landsat-7/8 data. The approach is implemented in four steps: i) partitioning the Landsat land surface temperature (LST) to derive the crop water stress coefficient (Ks), ii) estimating the daily root zone soil moisture (RZSM) from the integration of Landsat-derived Ks into a crop water balance model, iii) retrieving irrigation at the Landsat pixel scale and iv) aggregating pixel-scale irrigation estimates at the crop field scale. The new irrigation retrieval method is tested over three agricultural areas during four seasons and is evaluated over five winter wheat fields under different irrigation techniques (drip, flood and no-irrigation). The model is very accurate for the seasonal accumulated amounts (R ~ 0.95 and RMSE ~ 44 mm). However, lower agreements with observed irrigations are obtained at the daily scale. To assess the performance of the irrigation retrieval method over a range of time periods, the daily predicted and observed irrigations are cumulated from 1 to 90 days. Generally, acceptable errors (R = 0.52 and RMSE = 27 mm) are obtained for irrigations cumulated over 15 days and the performance gradually improves by increasing the accumulation period, depicting a strong link to the frequency of Landsat overpasses (16 days or 8 days by combining Landsat-7 and -8). Despite the uncertainties in retrieved irrigations at daily to weekly scales, the daily RZSM and evapotranspiration simulated from the retrieved daily irrigations are estimated accurately and are very close to those estimated from actual irrigations. This research demonstrates the utility of high spatial resolution optical and thermal data for estimating irrigation and consequently for better closing the water budget over agricultural areas. We also show that significant improvements can be expected at daily to weekly time scales by reducing the revisit time of high-spatial resolution thermal data, as included in the TRISHNA future mission requirements.

Keywords: Irrigation, Land surface temperature, FAO-56 model, Landsat, Root-zone soil moisture, Evapotranspiration.

1 Introduction

Irrigated agriculture consumes > 70% of freshwater at global scale (Foley et al., 2011) and > 80% in semi-arid and arid regions (Chehbouni et al., 2008; Garrido et al., 2010). The water scarcity issue is particularly acute in the Mediterranean, which is and will continue to be a hot spot of climate change with an observed trend towards warmer conditions and a greater irregularity in seasonal and annual precipitations (Giorgi, 2006; IPCC, 2013). Increasing the water use efficiency in agriculture is essential for the sustainability of water resources and hence has been identified as one key topic related to water scarcity and droughts (Werner et al., 2012). Despite the important pressure of agriculture on water resources, information on the amount of irrigated water is often unavailable. Therefore, monitoring and quantifying irrigation over extended areas is critical for an efficient management of water resources.

In an attempt to estimate the irrigation volumes from remote sensing data, some recent studies have explored the utility of surface soil moisture estimates from micro-wave sensors (Brocca et al., 2018, 2017; Escorihuela and Quintana-Seguí, 2016; Jalilvand et al., 2019; Kumar et al., 2015; Lawston et al., 2017; Malbéteau et al., 2018; Zhang et al., 2018). In particular, Brocca et al. (2018) developed an approach to quantify the irrigation amounts by combining the currently available coarse resolution satellite soil moisture products (e.g. SMAP, SMOS, ASCAT, AMSR-2) and a soil water balance. This work was applied over various semi-arid and semi-humid regions worldwide but could not be quantitatively assessed due to the unavailability of reliable in situ observations of irrigation over corresponding irrigated perimeters. However, this approach was quantitatively assessed at ~50 km resolution over a semi-arid region (Jalilvand et al., 2019). Some deficiencies were obtained over periods with sustained rainfalls and the method was not implemented in winter because the method fails in correctly separating irrigation from precipitation (Brocca et al., 2018). This makes the approach unsuitable for winter crops, which are especially important in the Mediterranean. Nevertheless, the ability to quantify monthly irrigations was demonstrated under specific conditions: during prolonged periods of low rainfall and using satellite soil moisture data with a low uncertainty and a frequency higher than 3 days.

There are two main issues with the use of microwave-based soil moisture for retrieving irrigation. The first limitation is the very coarse resolution (~40 km) of readily available satellite soil moisture data sets. The spatial resolution can be improved to 1 km resolution using disaggregation methods (e.g. Molero et al., 2016; Peng et al., 2017), but this enhanced resolution is still unsuitable for monitoring the water management at the crop field scale, i.e. about 100 m or 1 ha (Anderson et al., 2012). Furthermore, recent methods to obtain soil moisture data at suitable resolution (~100 m) have not reached an operational maturity yet (e.g. Amazirh et al., 2018; Merlin et al., 2013; Peng et al., 2017). The second limitation is related to the sensing depth (several cm or so) of microwave observations. The dynamics of the top soil moisture is likely to be used to detect irrigation events. However the volume sensed is much smaller than the root zone water storage, which weakens the capability of microwave-based approaches to solve the crop water budget.

Alternatively to microwave-based approaches, optical/thermal data have demonstrated to be valuable for monitoring the crop water requirements by means of evapotranspiration (ET) estimates (Gowda et al., 2008; Kalma et al., 2008; Li et al., 2009). Thermal data have the advantage over microwave data of providing information on the vegetation water status, even within individual fields, in order to improve the water use efficiency (Anderson et al., 2012). In this vein, different methods have been developed in the last decades to estimate ET from LST data (Gowda et al., 2008; Kalma et al., 2008; Li et al., 2009). Despite the large variety of existing approaches to estimate crop water requirements by means of ET estimates, irrigation is generally simulated from the modeled water needs (e.g. Allen et al., 1998; Bastiaanssen et al., 2007; Battude et al., 2017; Corbari et al., 2019; Duchemin et al., 2008). Those models are based either on the water balance or on the coupled energy-water balance, but in both cases, the simulated irrigation may differ considerably from actual irrigation amounts. The reason is that the modeling of soil moisture dynamics and its interaction with the crop consumption through ET is prone to significant uncertainties, especially when no information is available on the actual crop water status over time. Other approaches based on ET estimates from remote sensing surface energy balance (SEB) models (e.g. SEBS, SEBAL, METRIC) have the advantage of estimating the crop water requirement without the calculation of the water balance. This is feasible using daily optical/thermal data. The point is that the remotely sensed variables for operating SEB models at daily scale generally have a spatial resolution of 1 km or more (e.g. Romaguera et al., 2014; van Eekelen et al., 2015), which is unsuitable at crop field scale. When using high-spatial resolution optical/thermal data, the low temporal resolution has to be taken into account. In Droogers et al. (2010), a water balance model was calibrated to minimize the difference between simulated and remotely sensing Landsat-derived ET over an irrigated cotton crop field. The calibration involved adjusting the irrigation amount and a stress threshold below which irrigation is triggered. The stress threshold f_1 was defined as the actual to potential transpiration and ranged from 0.95 to 0.98 in that study. However, due to compensation effects between irrigation amounts and dates, the authors had to further constrain the inverse problem by fixing the irrigation dates during the first half of the season (from March to end of June) and to assume that there is no stress during the second half of the season (from July). Therefore, during the first stage, irrigation events are supposed to be known, while during the second stage, the approach in Droogers et al. (2010) is very similar to the application of the classical FAO-56 model (Allen et al., 1998) that triggers irrigation as soon as the root zone soil moisture gets below 0.95–0.98 times the critical soil moisture below which the crop stress starts. The retrieved irrigation amounts were assessed at the seasonal time scale but, due to the lack of validation data, they were not compared to actual irrigations at shorter time scales. Recently, Corbari et al. (2019) developed a system to predict the water needs (irrigation) from the coupling of remote sensing data, soil water-energy hydrological modeling and meteorological forecasts. Landsat-derived vegetation and albedo parameters, as well as land surface temperature (LST) data were used to initialize and calibrate the energy-water balance. However, this approach required observed data of the previous days (especially soil moisture) to simulate the soil moisture and irrigation water needs for up to 3 days, which is not currently possible over large scales because there is no method that allows obtaining operationally soil moisture data at suitable resolution (~100 m). Another approach was proposed by Chen et al. (2018) to detect the timing of irrigation from a vegetation index by using Landsat and MODIS reflectance data. The method was demonstrated to be promising in detecting irrigation events during the first half of the growing season only. Actually, vegetation index presents great fluctuation and is insensitive to water supplement during the second half of the growing season. In addition, the method does not allow retrieving irrigation amounts.

Among the thermal-based ET models, the contextual approaches have had an especial interest in the scientific community for its simplicity and operationality over large areas, by estimating ET as a fraction of either potential ET (Moran et al., 1994), or available energy (Long and Singh, 2012; Roerink et al., 2000). The evaporative fraction (EF, defined as the ratio of ET to available energy, i.e, the difference between net radiation and soil heat flux) can be estimated from the contextual information of remotely sensed optical and thermal images, where dry and wet conditions are identified from the LST – fv (e.g. Long and Singh, 2012; Moran et al., 1994) space, the LST – albedo (e.g. Roerink et al., 2000) space or even from their combination (Merlin, 2013; Merlin et al., 2014). According to a number of thermal-based methods, LST can be related to the root-zone soil moisture

(RZSM) by means of the canopy temperature and its associated transpiration (Boulet et al., 2007; Hain et al., 2009; Moran et al., 1994). Hence, one key step to estimate thermal-derived RZSM is the partitioning of LST into soil and canopy temperatures (Merlin et al., 2014, 2012; Moran et al., 1994). In dry and wet regimes where a thermal-based EF (or canopy temperature-based water stress index) is 0 and 1, respectively, LST is no more sensitive to RZSM. LST is hence useful only in a transitional regime where RZSM is strongly related to LST. In the transitional regime, the soil moisture ranges between a given critical soil moisture (SM_{crit}, below which vegetation is under stress condition) and the soil moisture at permanent wilting point (SM_{wp}, below which water is not accessible to plants). SM_{crit} is thus defined between SM_{wp} and the soil moisture at field capacity (SM_{fc}, above which water cannot be held against gravitational drainage). Therefore, the nonlinear response of LST for different RZSM levels/regimes is a big issue when trying to develop a RZSM retrieval approach from LST data. Olivera-Guerra et al. (2018) developed an approach to derive a first guess RZSM from a LST-derived water stress coefficient, while under unstressed conditions (i.e. when LST is no more sensitive to RZSM) the RZSM was estimated from a crop water balance model. The temporal dynamics of RZSM were hence obtained along the season under stressed and unstressed condition, by making an optimal use of both the water budget model and sequential LST observations. However, the method in Olivera-Guerra et al. (2018) was not applied to remote sensing data and its application to readily available LST observations requires to account for three major issues that are addressed in the present work. First, a contextual approach should be implemented from Landsat data to partition the LST into canopy and soil temperatures by detecting the wet and dry conditions from the LST – fv space. This would allow for estimating a Landsat-derived crop stress coefficient (Ks) over large scales. Second, a serious complexity is introduced when trying to estimate the daily RZSM from sparsely available Landsat data. Especially the Landsat-derived Ks should be integrated into a crop water balance model in both recursive and forward modes, in order to provide the temporal dynamics of RZSM along the season at pixel scale over large areas. Third, given that irrigation is usually applied within a single day over the entire crop field, the pixel-scale irrigation estimates can be aggregated (following a strategy to be defined) to provide the irrigation dates and amounts at the crop field scale.

Therefore, this study aims, for the first time, to develop an original approach to retrieve the crop field scale irrigation timing and amounts on a daily basis all along the agricultural season from readily available remote sensing data. For this purpose, a key and novel step in the approach is to estimate the daily RZSM by combining a forward and recursive crop water balance initialized by temporally-sparse Landsat data. To our knowledge it is the first remote sensing-based approach to estimate irrigation at such high spatio-temporal resolution from readily available optical/thermal data and without relying on ad hoc assumptions on irrigation regimes (e.g. no stress) and/or dates. The approach is implemented with Landsat-7 and -8 data over three 12 km by 12 km areas in central Morocco and is validated over five sites with different irrigation techniques (drip, flood and no-irrigation) during four agricultural seasons. The paper is presented as follows. Data sets are first described (Section 2). Next, the irrigation retrieval method is presented: i) partitioning the Landsat LST to derive the crop water stress coefficient Ks, ii) estimating the daily RZSM from the integration of Landsat-derived Ks into a crop water balance model, iii) retrieving irrigation at the Landsat pixel scale and iv) aggregating pixel-scale irrigation estimates at the crop field scale (Section 3). Then, the approach is tested over three agricultural areas and validated against in situ measurements in terms of irrigation as well as daily RZSM and ET (Section 4). Finally, the conclusions and perspectives are presented (Section 5).

2 Data collection and pre-processing

The study focuses on three 12 km by 12 km agricultural areas located in the semi-arid Haouz plain in central Morocco (Fig. 1). Each agricultural area is mainly covered by winter wheat crops. Five experimental sites comprising two drip irrigation, two flood irrigation and one rainfed wheat fields were monitored during four agricultural seasons. Details about irrigation systems, crop field area and monitoring period per area, named Chichaoua, R3 and Sidi Rahal are showed in Table (1). The soil texture are predominantly clay loam, clay and silt loam for Chichaoua, R3 and Sidi Rahal areas, respectively. The site of Sidi Rahal (Bour) was maintained under bare soil conditions during the 2015-2016 season due to the dry winter of 2015. However, the four seasons between 2015 and 2018 are used as benchmark. More details about the field campaigns can be found in Ait Hssaine et al. (2018), Amazirh et al. (2018, 2017), Merlin et al. (2018) and Rafi et al. (2019).

2.1 Ground-based data

2.1.1 Irrigation data

In the Chichaoua area, flowmeters were used to monitor the irrigation of the two drip-irrigated fields. Irrigation was applied every 3–4 days during the 2016–2017 season until mid-April. Nevertheless, one field (EC1) was voluntarily stressed during specific periods along the season (controlled stress). Irrigations were stopped at mid-March and at the beginning of February of the 2017–2018 season over the reference (EC2) and controlled stress (EC1) field, respectively. The mean irrigation was 13 mm over 2 h.

In the R3 area, the flood-irrigated fields were irrigated every 1 to 3 weeks from January to April. Irrigation of the 2 ha field was precisely measured with a mean irrigation of 33 mm distributed in 8 events, while the 4 ha field was irrigated 7 times with an estimated volume of 64 mm each. No irrigation was applied to the Sidi Rahal rainfed (Bour) wheat field.

2.1.2 Meteorological and flux stations

Automatic meteorological stations were installed in each experimental area: two over alfalfa fields close to the monitored wheat fields in the Chichaoua and R3 areas and one over the monitored rainfed wheat field in Sidi Rahal. Meteorological data including air temperature, solar radiation, relative humidity and wind speed were collected continuously every 30 min. Likewise, five micro-meteorological stations equipped with eddy-covariance systems were installed in each site. Here, net radiation was measured by NR01 (Hukseflux) or CNR (Kipp & Zonen) radiometers, depending on the station. Soil heat fluxes were estimated from two HFP-01 heat flux plates (Hukseflux) per site buried at 5 cm. Finally, latent and sensible heat fluxes were acquired with krypton KH2O hygrometers (Campbell) and CSAT3 3D Sonic Anemometers at a frequency of 10 Hz and averaged over 30 min. The reliability and quality of the eddy covariance measurements over each field have been assessed through the energy balance closure (Ait Hssaine et al., 2018; Amazirh et al., 2017; Rafi et al., 2019).

2.1.3 Soil moisture data

Time Domain Reflectometry (TDR) probes (CS615 and CS655) were installed near the flux stations in each site to measure the soil moisture at different depths. The TDR probes were installed at 5, 15, 25, 35, 50, 80 cm in the stress controlled drip-irrigated (Chichaoua) and in the 4 ha flood-irrigated field (R3). Meanwhile, the TDR probes were installed at 5, 15, 30, 50, 80 cm in the reference drip-irrigated field and in the 2 ha R3 flood-irrigated field. In the rainfed wheat field, the TDR probes were installed only at the soil surface layer (at 5 and 10 cm). The measurements at different depths were used to estimate the soil moisture integrated over the root zone by means of linear interpolations. In situ RZSM estimates were then normalized by using the soil moisture values at wilting point (SM_{wp}) and at field capacity (SM_{fc}) estimated from pedo-transfer functions (Wosten et al., 1999).

2.2 Remote sensing data

Landsat-7 and -8 data collected for the agricultural seasons from 2014 to 2018 are used. Images with <30% of cloud cover are considered for the analysis, giving an average of 20 images per agricultural season. We combine Landsat-7 and 8 to increase the frequency of the thermal data since it is one main critical issue for monitoring crop water use together with its high spatial resolution. We estimate LST and *fv* using both optical and thermal data (see below). We maintain the 30 m spatial resolution for all data, even when the thermal bands are resampled from their original 60 m and 100 m resolution for Landsat-7 and -8, respectively.

2.2.1 Land surface temperature

LST is estimated using the single-channel algorithm described in Jiménez-Munoz et al., (2009, 2014), which uses as input the thermal band of Landsat, the atmospheric water vapor content, and the spectral surface emissivity. The thermal data are acquired from bands 6 and 10 of Landsat-7 and -8 Level-1, respectively, while the atmospheric water vapor content is obtained from the daily MODIS MOD05 v6.0 product. The spectral surface emissivity is estimated using the simplified NDVI thresholds method proposed by Sobrino et al., (2008), which weights the spectral soil and vegetation emissivity (here set to 0.985) through the *fv*. Similarly, the spectral soil emissivity is obtained from the ASTER GED product by using bands 13 and 14 with the above-mentioned simplified NDVI method. Then, the ASTER spectral soil emissivities are adjusted to the Landsat thermal bands using the broadband regression approach (Ogawa and Schmugge, 2004) as in Malakar et al., (2018) and Duan et al. (2018). The regression coefficients between the emissivities for Landsat and ASTER bands were derived by convoluting the soil emissivity spectra of all soil types available in the ASTER spectral library for every thermal band (Baldridge et al., 2009). Accuracies resulted in root mean square error (RMSE) of 0.0007 and 0.0005, and R^2 of 0.96 and 0.99 for Landsat-7 and -8 thermal band, respectively. The reliability of LST estimates was assessed in Amazirh et al. (2019, 2017), which found a relatively good agreement between satellite and ground-based LST over the sites of the study area with a RMSE lower than 2.4 K.

2.2.2 Fractional green vegetation cover

The fractional green vegetation cover *fv* is estimated linearly between a minimum and maximum of the Normalized Difference Vegetation Index (NDVI), which often represent bare soil (NDVIs) and fully vegetated surface (NDVIv) values, respectively (Gutman and Ignatov, 1998). NDVIs and NDVIv are set to 0.14 and 0.93 (Duchemin et al., 2006). NDVI values are estimated using the red and near-infrared bands of Level-2 Landsat products.

3 Method

The method to retrieve irrigation dates and volumes from Landsat LST/NDVI time series is described below. The basic idea behind the retrieval approach is first to determine the irrigation date and then to estimate the (daily) irrigation amount as the difference between the RZSM estimated on the irrigation date and that estimated on the day before. As in Olivera-Guerra et al. (2018), thermal-derived crop stress coefficient (Ks) is translated into RZSM diagnostic by means of the dual crop coefficient FAO (FAO-2Kc) formalism. In this former work, irrigation was estimated from the variability in daily first guess RZSM by using optical/thermal in situ observations. Given that the method proposed herein uses temporally sparse Landsat data, the Landsat-derived RZSM diagnostic is propagated in a recursive and forward water balance mode to estimate the daily RZSM along the season. Therefore, this method significantly differs from the study in Olivera-Guerra et al. (2018) in several major aspects. For clarity, the main assumptions are listed (Section 3.1) and each original component is described separately: the irrigation retrieval at the pixel scale using Landsat-derived Ks (Section 3.2), the use of a contextual method to derive RZSM from Landsat data (Section 3.3), the implementation of a crop water balance model (WB) in recursive and forward modes to estimate the daily RZSM between two successive Landsat overpass dates (separated by 8 to 16 days in clear sky conditions) (Section 3.4), the aggregation of pixel-scale irrigation estimates at the crop field scale (Section 3.5), and the definition of a validation strategy of the field-scale retrieved irrigation dates/volumes (Section 3.6).

3.1 Model assumptions

The approach is based on several assumptions, some of which relate to the FAO-2Kc modeling approach, while others are specific to the proposed irrigation retrieval method. The assumptions deriving from the FAO-2Kc model are:

- The daily RZSM varies within a range defined by a minimum value set to the soil moisture at wilting point (SM_{wp}) and by a maximum value set to the soil moisture at field capacity (SM_{fc}). Both extreme soil moisture values are estimated using pedo-transfer functions (Wosten et al., 1999). SM_{wp} and SM_{fc} were equal to 0.17 and 0.32 m^3m^{-3}, respectively. Uniform soil parameters were used to test the genericity of the irrigation retrieval approach.

- When RZSM reaches SM_{fc}, any additional water supply is considered as water excess and is therefore drained from the soil bucket by deep percolation (occurring simultaneously to the water excess supply).
- The RZSM is linearly related to Ks between SM_{wp} and the critical RZSM (SM_{crit} = 0.24 m^3m^{-3}), which is estimated as a fraction of the total available water (i.d. difference between SM_{fc} and SM_{wp}) according to the water stress tolerance of crops (Allen et al., 1998).
- The rooting depth is estimated from the vegetation cover and varies linearly between a minimum value (set to 0.1 m) and a maximum value depending on the crop type.

The assumptions specific to the irrigation retrieval approach are:

- The retrieved irrigation is the effective irrigation (irrigation minus drainage), meaning that the irrigation excess which triggers deep percolation is not taken into account.
- An irrigation event is detected on the day when the RZSM estimated recursively from the FAO-2Kc water budget reaches SM_{fc} and it is not due to rainfall.
- The field-scale retrieved irrigation occurs on the same day over the entire field crop.
- Due to the saturation of Landsat-derived Ks (equal to 1) for soil moisture values between SM_{crit} and SM_{fc}, the Landsat-derived RZSM ranges between SM_{wp} and SM_{crit}.

- If two successive Landsat overpass dates both indicate unstressed conditions (Ks=1), it is assumed that the crop does not undergo water stress during that period. It is also assumed that Ks=1 between a Landsat date indicating unstressed conditions and an irrigation event detected before the next Landsat overpass date.
- In our study, the capillarity rise and runoff are neglected due to flat surfaces and a water table significant deep (>30 m) in the study area (Duchemin et al, 2006

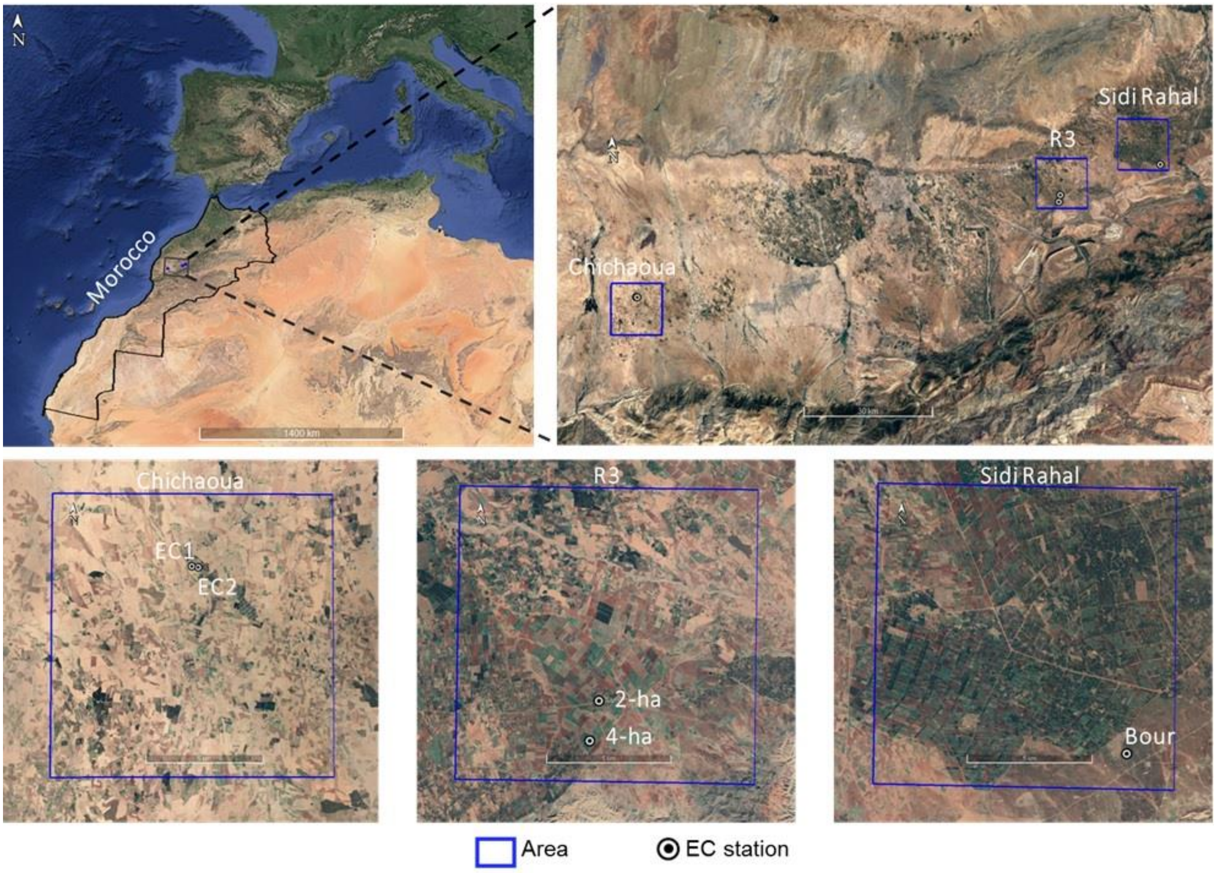

).

3.2 Pixel-scale irrigation retrieval

Irrigation is first estimated at the Landsat pixel scale as:

$$I_i = 1000(RZSM_i - RZSM_{i-1})Zr_i \quad (1)$$

where I_i is the irrigation amount (mm) on the irrigation date *i* and $RZSM_i$ and $RZSM_{i-1}$ (m^3/m^3) the RZSM estimated on the irrigation day and on the day before, respectively. The RZSM unit (m^3/m^3) is converted to irrigation depth (mm) by the factor $1000Zr_i$, with Zr_i being the effective root zone depth (m) at the irrigation date. Zr_i is estimated according to the Appendix A.1.

To estimate $RZSM_i$ in Eq. (1), the WB is applied in the recursive mode (here-after referred to as RWB) at daily scale for every period between two consecutive clear sky Landsat overpass dates (*j* and *j-Pj,* with *Pj* being the number of days between both successive Landsat dates). The RWB is applied from the last Landsat overpass date of the season to its previous dates. Therefore, the RWB is initialized at date j (j > i) from a Landsat-derived RZSM ($RZSM_{Landsat,j}$), and an irrigation event is detected at date i when the simulated $RZSM_{RWB,t}$ (for t = j-1, …,i) reaches SM_{fc}. However, four different cases need to be considered depending on the value (equal or smaller than 1) of Landsat-derived Ks at dates *j-Pj* and *j*. For clarity, each case is illustrated in Fig. *2*.

Case 1. stressed-stressed (Fig. *2*.a). The crop is under stress (Ks < 1) on both Landsat overpass dates j and j-Pj. Hence both $RZSM_{Landsat,j}$ and $RZSM_{Landsat,j-Pj}$ are smaller than SM_{crit}. In this case, if an irrigation event at date *i > j-Pj* (i.e. $RZSM_{RWB,t} = SM_{fc}$) is detected, the WB model is used in the forward mode (referred to as FWB) to estimate the RZSM at day *i-1* from an initial value set to $RZSM_{Landsat,j-Pj}$. The irrigation amount at date *i* is estimated as:

$$I_i = 1000\left(SM_{FC} - RZSM_{FWB,t=i-1}\right)Zr_i \qquad (2)$$

Case 2. stressed-unstressed (Fig. *2*.b). The crop is under stress (Ks < 1) on Landsat overpass date j-Pj and is unstressed (Ks = 1) on Landsat overpass date j. In this case, the RWB is initialized to SM_{crit} at Landsat overpass date j and if $RZSM_{RWB,t=i}$ reaches SM_{fc} for $i > j\text{-}P_j$, then $RZSM_{t=i-1}$ is estimated from the FWB initialized by $RZSM_{landsat,j-Pj}$ at Landsat overpass date *j-Pj*. The irrigation amount is then estimated as in Eq. (2).

For cases 1 and 2, two other specific conditions need to be considered:

i) $RZSM_{FWB,t}$ might reach its minimum value (SM_{wp}) before the detected irrigation event from $RZSM_{RWB,t=i}$. In that situation, another irrigation event is triggered in such a way that the simulated $RZSM_{FWB}$ is set to SM_{fc} and the FWB is used to propagate RZSM until *i-1* in the Eq. (2).

ii) $RZSM_{RWB,t}$ does not reach SM_{fc} for $t > j\text{-}Pj$. In that case, an irrigation is detected at date j-Pj + 1 provided that the difference between $RZSM_{RWB,j-Pj+1}$ and $RZSM_{Landsat,j-Pj}$ is positive and significant (larger than a given threshold to be set). In this case, the irrigation amount is calculated as:

$$I_{i=j-Pj+1} = 1000\left(RZSM_{RWB,i} - RZSM_{Landsat,j-P_j}\right)Zr_i \qquad (3)$$

Note that the threshold is determined as the uncertainty associated to $RZSM_{Landsat,j-Pj}$ estimate by using the propagation of uncertainty method from the partial derivatives of every independent variable (see Appendix A.2).

Case 3. unstressed-stressed (Fig. *2*.c). The crop is unstressed (Ks = 1) on Landsat overpass date j-Pj and is under stress (Ks < 1) on Landsat overpass date j. In this case, if an irrigation event at date $i > j\text{-}Pj$ (i.e. $RZSM_{RWB,t}=SM_{fc}$) is detected, then $RZSM_{t=i-1}$ is set to SM_{crit} at date *i-1*. The irrigation amount at date *i* is thus determined as follows:

$$I_i = 1000\left(SM_{fc} - SM_{crit}\right)Zr_i \tag{4}$$

Case 4. unstressed-unstressed (Fig. *2*.d). The crop is unstressed (Ks = 1) on both Landsat overpass dates j-Pj and j. In this case, an irrigation is detected (date) and estimated (amount) as in the Case 3.

For cases 3 and 4, $RZSM_{Landsat,j\text{-}Pj}$ is updated by $RZSM_{RWB,j\text{-}Pj}$. The updated RZSM at j-Pj is then used to reinitialize the previous period (from date *j-Pj* to its previous Landsat overpass date).

3.3 Landsat-derived RZSM

The Landsat-derived RZSM ($RZSM_{landsat,j}$) is estimated as:

$$RZSM_{landsat,j} = SM_{wp} + Ks_{Landsat,j}\left(SM_{crit} - SM_{wp}\right) \tag{5}$$

where $Ks_{Landsat,j}$ is the Landsat-derived Ks, estimated from a normalization of the Landsat-derived vegetation temperature (Tv), using minimum (Tv_{min}) and maximum (Tv_{max}) Tv values. Hence, Ks values range between 0 and 1, where 1 corresponds to well-watered/unstressed vegetation ($Tv = Tv_{min}$) and 0 to non-transpiring or senescent vegetation ($Tv = Tv_{max}$). Landsat-derived Tv is obtained from a partitioning method of LST:

$$Tv = \frac{LST - (1 - fv)Ts}{fv} \qquad (6)$$

with Ts being the soil temperature and fv the fractional vegetation cover. This partitioning method is based on the LST-fv feature space (e.g. Jiang and Islam, 2003; Long and Singh, 2012; Merlin et al., 2014; Sandholt et al., 2002), by incorporating the assumptions of the two-source surface energy balance (TSEB) formalisms (Norman et al., 1995). First, the LST-fv feature space is used to estimate the temperature endmembers (Tv_{min}, Tv_{max}, Ts_{min} and Tv_{max}) from a polygon constrained by a "dry edge" (defined as the line between Ts_{min} and Tv_{min}) and a "wet edge" (defined as the line between Ts_{max} and Tv_{max}). The "wet edge" and "dry edge" are determined from the linear regressions of the minimal and maximal LST, respectively, which are selected by *fv* classes with an interval of 0.01 (see Fig. 3.a). Second, the TSEB assumption for solving the vegetation and soil fluxes components and their corresponding Tv and Ts is only used for the partitioning of LST by applying Eq. (6). The procedure is initialized with Tv being equal to Tv_{min} and the corresponding initial Ts by decomposing linearly the LST from Eq. (6). This is consistent with the TSEB approach when the transpiration rate is initialized to its potential rate (corresponding to $Tv = Tv_{min}$). If Ts is above the Ts_{max}, Ts is then set to Ts_{max} and a new Tv is calculated from Eq. (6). In that case, the vegetation undergoes water stress ($Tv > Tv_{min}$). Therefore, the TSEB assumption in the LST-fv feature space (see Fig. 3.b) makes Tv equal to Tv_{min} for every Ts below Ts_{max}, while Ts remains equal to Ts_{max} when Tv is larger than Tv_{min}.

3.4 Water balance-derived RZSM

The daily RZSM between Landsat overpass dates is estimated by solving the crop WB in forward and recursive modes, named FWB and RWB respectively. According to the FAO-2Kc formalism, the general expression of the crop WB model is:

$$Dr_t = Dr_{t-1} + ET_t - P_t - I_t + DP_t - CR_t + RO_t \tag{7}$$

where Dr is the root zone depletion, ET the evapotranspiration, P the precipitation, DP the deep percolation, CR the capillarity rise, RO the surface runoff and I the irrigation. Every term is expressed in mm for the day *t* (and *t-1* for Dr). According to the assumptions used in this study, CR and RO are neglected while I is the variable to be estimated. Therefore, the FWB and RWB models can be expressed in Eqs. (8) and (9), respectively as:

$$Dr_t = Dr_{t-1} + ET_t - P_t \tag{8}$$

$$Dr_{t-1} = Dr_t - ET_t + P_t \tag{9}$$

Note that in the above equations, the DP resulting from heavy rainfall is not computed since Dr_t or Dr_{t-1} are set to 0 when $P_t > Dr_{t-1} + ET_t$ or $P_t > Dr_t - ET_t$ for FWB and RWB, respectively. For both RWB and FWB models, the Landsat-derived RZSM (either $RZSM_{Landsat,j-Pj}$ or $RZSM_{Landsat,j}$) is used to initialize the root zone depletion.

$$Dr_t = 1000(SM_{fc} - RZSM_t)Zr_t \tag{10}$$

In Eqs. (8) and (9), ET_t is estimated from the FAO-2Kc formalism, where its basal crop coefficient (Kcb) and evaporation coefficient (Ke) are estimated from a generic expression from the daily *fv* interpolated from Landsat data. More details about the generic expressions to estimate Kcb and Ke are described in Appendix A.3. Kcb and Ke are first adjusted using Ks and an evaporation reduction coefficient (Kr), which are initialized from their Landsat-derived estimates (at date *j-Pj* or *j* for forward or recursive mode, respectively). Then Ks and Kr are computed from the crop WB according to FAO-2Kc. Similarly to Ks, Kr is estimated as the normalization of Ts between Ts_{min} and Ts_{max}. Finally, RZSM in forward ($RZSM_{FWB,t}$) and recursive ($RZSM_{RWB,t}$) modes are obtained from the root zone depletion by inverting Eq. (10).

3.5 Crop field scale irrigation retrieval

The irrigation was previously retrieved from the RZSM derived at the pixel level regardless of its neighboring context. Hence the within-field variability in terms of predicted irrigation dates and amounts can be further constrained. Given that irrigations usually occur on the same day over the entire crop field, we propose a procedure of aggregation to provide the irrigation dates and amounts at the crop field scale. The three-step procedure is described below.

First, for each period P_j between two successive satellite overpasses, the number of irrigations within a given crop field ($N_{Ifield,Pj}$) is estimated as the total number of irrigations at pixel-scale divided by the number of pixels contained in the crop field (N_{pixel}). Then, the daily amounts of irrigation at pixel-scale are averaged within the crop field (I_i). The daily fraction of irrigated pixels (f_i) is also estimated as the number of pixels where irrigation is detected divided by N_{pixel} (Fig. 4). Finally, the irrigation volume applied over the crop field (I_{field}) is estimated by integrating the amounts of irrigation in the $N_{Ifield,Pj}$ sub-periods of period P_j (Eq. 11). The most probable date ($Date_{Ifield}$) of the irrigation event within each sub-period is estimated similarly according to Eq. (12).

$$I_{field} = \frac{\int_{ini}^{end} I_i f_i d_i}{\int_{ini}^{end} f_i d_i} \tag{11}$$

$$Date_{Ifield} = \frac{\int_{ini}^{end} i I_i f_i d_i}{\int_{ini}^{end} I_i f_i d_i} \tag{12}$$

with I_i and f_i being the areal averaged irrigation and the fraction of irrigated pixels within the field crop on day i, respectively. d_i is the time differential in the integral equations. The limits of integration *ini* and *end* are set according to f_i and $N_{Ifield,Pj}$ in period P_j. $N_{Ifield,Pj}$ is equal to the number of local maxima (peaks) of f_i detected for each sub-period. The limits *ini* and *end* are set to the first day before and the last day after the peak with f_i is equal to zero (i.e. the days when irrigation is not detected in any pixel of the field), respectively. For clarity, different integration periods are illustrated in Fig. 4.

3.6 Validation strategy

3.6.1 Irrigation

The performance of the irrigation retrieval method is evaluated at various time scales. In order to do that, the irrigation amounts are accumulated in overlapping windows throughout the seasons by increasing sequentially the windows from 1 day to 3 months

(90 days). This strategy is implemented for every site. It allows the performance of the approach to be assessed for different accumulation periods, to be compared with the temporal resolution of Landsat data. The total irrigation applied during the entire season is also evaluated for all the sites.

The retrieved irrigation is also compared against the classical approach, which assumes no stress, meaning that irrigation is triggered when the RZSM reaches SM_{crit} in order to maintain Ks at 1. For this purpose, FAO-2Kc is run to simulate irrigation events along the season in order to maintain the crop under unstressed conditions (here-after referred to as FAO-$2Kc_{Ks=1}$). Note that the coefficients used in the FAO-2Kc (Kcb and Ke) are also averaged within the crop field, consistent with the irrigation retrieval method. The deep percolation resulting from the actual irrigation (I_{obs}) is removed from the comparison because our approach and FAO-$2Kc_{Ks=1}$ both estimate the effective irrigation only (i.e. without deep percolation resulting from irrigation). For this purpose, the deep percolation is estimated according to the FAO-2Kc forced by actual irrigation (here-after referred to as FAO-$2Kc_{Iobs}$).

3.6.2 RZSM and ET

The irrigation retrieval method is also assessed in terms of RZSM and ET estimates. Indeed, RZSM is an intermediate variable from which irrigation is retrieved, and ET is indirectly related to the irrigation through the RWB and the FWB. For this purpose, the retrieved irrigation is used to force FAO-2Kc to simulate RZSM and ET on a daily basis, and the RZSM and ET estimates are compared with in situ observations. The results are notably compared with those obtained for the FAO-$2Kc_{Iobs}$ (in situ irrigation) and FAO-$2Kc_{Ks=1}$ (no stress) approaches. In summary, the validation strategy implies running the

FAO-2Kc by using the water balance driven by i) the actual irrigation, ii) the irrigation simulated without stress (Ks = 1) and iii) the retrieved irrigation from our approach.

4 Results and discussions

The irrigation retrieval is applied to the four irrigated sites and to the rainfed site. Results are assessed in terms of the retrieved irrigation amount and timing, and in terms of the intermediate variables (RZSM and ET) needed in the irrigation retrieval algorithm.

4.1 Irrigation

Fig. 5 shows the comparison between the irrigation retrieved by the proposed methodology ($I_{FAO\text{-}2Kc\_Landsat}$), the irrigation simulated by FAO-2Kc by avoiding stress ($I_{FAO\text{-}2Kc\_Ks=1}$) and the actual irrigation (I_{obs}). The comparison is carried out for each site and season separately. Over flood-irrigated wheat fields in R3 area, six and five irrigation events are correctly estimated in the R3-4ha and R3-2ha field, respectively, against the seven and eight irrigations that were actually applied by the farmer. Note that the irrigation applied at the end of the development stage (equal to 64 and 36 mm in R3-4ha and -2ha, respectively) is missing over both sites. It could not be detected by the retrieval approach due to a virtual increase in the WB model of the root zone storage associated with the root growth. Thus, according to the WB model, no irrigation is needed in this period to supply the crop water needs. In R3-2ha field, three irrigation events are retrieved during the mid-season stage instead of the five irrigations applied by the farmer in the same period. That is because of i) the cloud-free Landsat data are widely separated (by 16 and 24 days) during this period and ii) the approach assumes a maximum irrigation amount by fully filling up the water storage capacity while the actual irrigations possibly do not reach this threshold and hence the number of retrieved irrigation events is generally reduced. The latter also explains the overestimation of irrigation amounts by event during the mid-season stage over both R3-4ha and R3-2ha fields. Indeed, in both sites, the irrigation amount estimated in the initial stage (i.e. beginning of the growing season) was much underestimated compared to the irrigation really applied by farmers. Regarding the irrigation dates in R3-4ha field, three first irrigation events are accurately detected with a time difference about the actual events shorter than 3 days, while the last three irrigation events are poorly estimated with a time difference of about one week. The precision in the timing of retrieved irrigations is also closely linked to the frequency of cloud-free Landsat data over the crop field since the first irrigations are detected with an availability of Landsat data every 8 days, while the last irrigations are detected by using cloud-free images separated by 40 and 24 days. The difference between observed and retrieved irrigation (date and amount) may be also related to the inadequate amount and planning of irrigation by the farmer. In fact, irrigation amounts and timing are planned only by the understanding and perception of the farmer without using any guideline for scheduling the amount and timing of irrigation water applications. Consequently, some irrigations are missing and some are unnecessary.

Similarly, in Chichaoua area over both sites (EC-1 and EC-2) and seasons (2016-2018), the irrigations in the initial stage are underestimated while in the mid-season stage the amount by irrigation event is much overestimated. As it was mentioned for R3 fields, the fact that the FAO-based approach simulates water supplies by filling up the water storage capacity makes the amounts be modulated by the water storage capacity, which depends on the rooting depth Zr and the parameterization for soil properties and vegetation type (i.d. SM_{wp}, SM_{fc} and SM_{crit}). Consequently, during the initial stage when Zr is equal or close to its minimum value (set to 0.1 m) the water supplies to fill up the root zone are smaller while they are larger during the mid-season stage when Zr is close to 1 m. Moreover, as it is observed in all irrigated fields, applying large amounts of water supplies during initial stages is a common irrigation practice applied by the farmers, on the one hand, in order to store water in layers deeper than the actual root zone at the initial stage and, on the other hand, to avoid the appearance of soil crusting thus facilitating the plant emergence (Le Page et al., 2014). This is not taken into account in the proposed approach. Specifically over the drip-irrigated fields, the overestimation in irrigation amounts is partially explained by i) the irrigation frequency operated by the farmer (1-3 days), which is much higher than the Landsat temporal resolution (> 8 days) and ii) the small amounts applied without completely fill up the reservoir storage capacity (i.e. the RZSM does not necessarily reach the SM_{fc} after each irrigation). Regarding the stressed periods in EC1 site during the growing season 2016-2017, no irrigation was applied during the periods from DAS 68 to 97 and from DAS 101 to 114. In coherence, no irrigation is detected by our approach during the period DAS 68 to 97. However, an irrigation event of 49 mm is detected on DAS 106, which might represent two irrigations of 43 mm applied by the farmer one week before. Conversely in the EC2 field during the growing season 2016-2017, the farmer applied 8 irrigation events with amounts smaller than 10 mm every 2 days during two periods from DAS 77 to 81 and from DAS 87 to 95. During these two periods, our approach was able to detect one irrigation per period with amounts of 33 and 38 mm, respectively. These amounts are much larger than those applied by the farmer but they are together very close to the irrigation accumulated during both periods (68 mm).

In Sidi Rahal area, the rainfed wheat field is used as benchmark to evaluate where no irrigation should be retrieved. Only three significant irrigation events are detected in the 2014-2015 and 2017-2018 seasons while in the other seasons some irrigation events are estimated but with very small amounts lower than 15 mm. In the mid-season stage of the 2014-2015 season, two important irrigation events (31 and 38 mm) are retrieved from a significant difference between $RZSM_{RWB,j-Pj+1}$ and $RZSM_{Landsat,j-Pj}$ at date *j-Pj+1* (situation (ii) of case 1 or 2). In this period between Landsat overpass dates, the water depleted from the crop consumption through ET minus the precipitation (according to the WB) is much larger than the difference of $RZSM_{Landsat}$ between dates *j* and *j-Pj*, which is thus translated in the retrieved irrigation amounts. That is partially explained by uncertainties in the estimation of ET, the water storage capacity (from SM_{wp}, SM_{fc} and Zr) or capillarity rises from deeper layers that are neglected in the approach.

Despite the differences between daily retrieved and actual irrigation, the proposed approach is able to accurately estimate the total irrigation amount applied at the seasonal time scale (see Fig. 6) with a correlation coefficient (R) equal to 0.95, a RMSE of 44 mm and a bias lower than 15 mm. Fig. 6 shows also the comparison with the classical approach FAO-$2Kc_{Ks=1}$, which provides poor estimates of irrigations due to a large overestimation (bias=252 mm). Such an overestimation is explained by that fact that the FAO-$2Kc_{Ks=1}$ approach avoids the water stress, regardless of the crop water status. Following FAO-$2Kc_{Ks=1}$, the winter wheat fields would need between 300 and 400 mm by season, while both the irrigation applied by farmers and the retrieved irrigation were very different by field and by season. It should be noted that in bare soil conditions (Bour 2015-2016), FAO-$2Kc_{Ks=1}$ estimates several irrigation events of small amounts. This is due to the top surface soil layer (set to 10 cm) that is quickly depleted by evaporation and needs to be re-filled frequently to maintain the Ks equal to 1. Note that the FAO-based approach assumes a minimum rooting depth (Zr_{min} set to 10 cm) even if there is no vegetation along the season. The root zone depletion and Ks are thus estimated in such conditions. As result, the total irrigation depth for Bour 2015-2016 season simulated by FAO-2$Kc_{Ks=1}$ is almost twice the wheat water requirements. The large simulated irrigation is also partly due to the low rainfall during this season and, consequently, the water balance requires larger water supply to maintain the Ks equal to 1. Over EC1 and EC2 fields in the 2016-2017 season, FAO-2$Kc_{Ks=1}$ obtained a total irrigation very close to that applied by the farmer because these sites were maintained unstressed during almost all the season.

A more comprehensive comparison at different time scales between the irrigation estimates from the classical approach FAO-2$Kc_{Ks=1}$ and the proposed approach FAO-2$Kc_{Landsat}$ is shown in *Fig. 7* . The irrigation amounts throughout the seasons are cumulated in overlapping windows of 1 day to 3 months (90 days). Overall, the proposed approach obtains a better performance than that of FAO-2$Kc_{Ks=1}$ with higher accuracies in term of R, bias and relative RMSE (RRMSE). With exception of two fields in Chichaoua area for 2017-2018 season, good agreements are reached over 15 days (R = 0.52 and RMSE = 27 mm) and then the agreements are further improved by increasing the accumulation period. Results for the fields in Chichaoua area for 2017-2018 season are relatively poor. This is mainly due to the stopping of irrigations early in the season (beginning of February for EC1 and mid-March for EC2) so that the water requirements were fulfilled mainly from the water stored in the soil or capillarity rise while the approach estimates significant irrigation amounts during that period. This problem can be partially explained by uncertainties and biases in the parameter values used to estimate the water storage capacity (SM_{wp}, SM_{fc} and Zr) and the capillarity rises from deeper layers that are neglected in the approach. Nevertheless, in spite of difficulties with monitoring drip irrigation, our approach has a better performance than the classical approach at every time scale, especially in terms of bias and RRMSE.

The results at different time scales indicate that the Landsat-based retrieval approach is robust for time intervals equal of longer than 2 weeks, which is the time period of Landsat acquisitions (~16 days). On the contrary, the approach generally fails in retrieving reliable cumulated irrigation for time periods shorter than 10 days by using the Landsat frequency. Therefore, we can expect significant improvements in the irrigation estimates at daily to weekly time scale by increasing the revisit frequency of LST data. Such high spatio-temporal resolution will be achieved by future thermal missions like TRISHNA (Lagouarde and Bhattacharya, 2018) .

4.2 Daily RZSM and ET

Fig. 8 and Table 2 report the results of the irrigation retrieval approach in terms of daily RZSM in comparison with the classical approach FAO-2Kc$_{Ks=1}$ and the FAO-2Kc forced by actual irrigations (FAO-2Kc$_{Iobs}$). The daily RZSM simulated from FAO-2Kc$_{Iobs}$ obtains an overall R equal to 0.75 and a RMSE equal to 0.04 m^3/m^3, while the proposed approach obtains an R slightly lower (0.66) and the same RMSE value. FAO-2Kc$_{Ks=1}$ obtains a low R equal to 0.25 and a RMSE of 0.07 m^3/m^3, meaning a deterioration of about 65% with regard FAO-2Kc$_{Iobs}$. The similar performance between the proposed approach and FAO-2Kc$_{Iobs}$ demonstrates that the retrieved irrigation is correctly estimated in order to simulate the RZSM temporal dynamics similar to that retrieved from the FAO-2Kc forced by actual irrigations.

Similarly, *Fig. 9* and *Table 3* show the comparison between the proposed approach, FAO-2Kc$_{Iobs}$ and FAO-2Kc$_{Ks=1}$ in terms of daily ET. Overall, the proposed approach provides better performance than FAO-2Kc$_{Ks=1}$ and is very close to the FAO-2Kc$_{Iobs}$. However, particular results were obtained in the Chichaoua fields (EC1 and EC2). For 2016-2017 season, the FAO-2$Kc_{Ks=1}$ obtains better results than the proposed approach due to the Ks simulated from actual irrigations is equal to 1 during almost all the season while the Landsat-derived Ks detects stressed conditions ($Ks_{Landsat} < 1$) during a large period in mid-season. In the 2017-2018 season, the proposed approach provides the best performance while results from FAO-2Kc_{Iobs} are worse than the others. Since the three FAO-based models differ only in the irrigation to force the WB by using the same parameterization, the fact that FAO-2Kc_{Iobs} obtains worse results confirms that over both sites the estimation of the water storage capacity and the capillarity rise is wrongly considered. This is also revealed during the mid-season stage when actual irrigation was stopped. Hence the irrigation retrieved by the proposed approach and by FAO-2$Kc_{Ks=1}$ during the mid-season stage compensates a too large water storage capacity or the (neglected) input of water from capillarity rise.

Note that FAO-2$Kc_{Ks=1}$ tends to overestimate the low ET rates typical of initial stages when the low vegetation cover makes the surface layer be quickly depleted by evaporation. In this stage, the top surface soil layer (set to 10 cm) is equal or very close to the root zone. The water storage after being depleted by evaporation, needs to be frequently re-filled to maintain the RZSM above the SM_{crit} (Ks = 1) by triggering irrigations and the evaporation is thus maintained at maximum rate. This can be clearly observed in Bour site, with longer initial stages and particularly throughout the 2015-2016 season, when soil remained bare all the season.

Finally, the high accuracy in ET estimates from the proposed approach and from FAO-2Kc_{Iobs} demonstrate the reliability of generic coefficients Kcb and Ke to be implemented with satellite data to estimate accurately ET at field scale over extended areas. The formulation of generic coefficients derived analytically (see Appendix A.3) from the link between the FAO-2Kc and a one source image-based model (SSEBop) allows avoiding calibration from in situ data that are rarely available over extended areas. Those generic coefficients would allow this implementation over different crop types although an extensive evaluation would be recommended.

4.3 Sensitivity analysis for soil parameters

The three main soil parameters (SM_{fc}, SM_{wp}, Zr) directly affect the water storage capacity and hence the estimation of the irrigation amount and timing. Note that SM_{crit} also affects the detection of irrigations and their amount particularly during unstressed periods (see Fig. 2). However, SM_{crit} is estimated from SM_{fc} and SM_{wp} and thus its impact is indirectly taken into account with SM_{fc} and SM_{wp}. SM_{crit} also depends on the crop tolerance to stress (fraction p) but as in Olivera-Guerra et al. (2018), the fraction p was considered constant for simplicity and because there is no significant difference for when using a constant or variable p (the variation in the overall RMSE and R^2 of simulated versus observed ET was found to be lower than 1%). Consequently, the sensitivity analysis is conducted for SM_{fc}, SM_{wp} and Zr only to assess the impact of uncertainties in soil parameters.

Fig. 10. Sensitivity analysis results for the soil parameters SM_{fc} and SM_{wp} by setting Zr_{max} set to 1.0 m. The irrigations are estimated by using SM_{fc} ranging between 0.28 and 0.40 m^3m^{-3} and SM_{wp} ranging between 0.10 and 0.24 m^3m^{-3}. The statistical parameter R (top) and RMSE (bottom) for actual irrigation accumulated over 15 days are estimated by using FAO-$2Kc_{Ks=1}$ (left) and FAO-$2Kc_{Landsat}$ (right) models. The red square indicates the SM_{fc} and SM_{wp} used in the approach.

depicts the sensitivity analysis for SM_{fc} and SM_{wp} in terms of retrieved irrigation by using the FAO-2Kc$_{Ks=1}$ and FAO-2Kc$_{Landsat}$ models over the site R3-4ha. The irrigation at daily scale are cumulated over 15 days and compared against cumulated actual irrigations. When looking at the variability of R and RMSE for irrigations from FAO-2Kc$_{Ks=1}$ and FAO-2Kc$_{Landsat}$, the later model is less sensitive to the soil parameters. The plots indicate that several optimal values can be found. This is due to the difference between SM_{fc} and SM_{wp} rather than the absolute value of each. Thus, the approach is sensitive to the water storage capacity defined by the difference between SM_{fc} and SM_{wp}, weighted by the root zone depth or in other words to the total available water (TAW = $Zr(SM_{fc} - SM_{wp})$). The higher R values of irrigation retrieved from FAO-2Kc$_{Landsat}$ suggest that the optimal difference ($SM_{fc} - SM_{wp}$) is between 0.17 and 0.19 m^3m^{-3}, consistent with the values proposed by Allen et al. (1998) for clayey soils. However in this study, SM_{fc} and SM_{wp} are set to 0.32 and 0.17 m^3m^{-3} respectively. Therefore, the approach can obtain a better performance by using optimal SM_{fc} and SM_{wp} values.

The root zone depth, which is estimated following the Appendix A.1, is also an important parameter in the water storage capacity. In the Eq. (A.1), the main parameter to be calibrated is Zr_{max}. Therefore, the same sensitivity analysis as for SM_{fc} and SM_{wp} was performed by using a Zr_{max} ranging from 0.5 to 1.5 m. These Zr_{max} values are typical for wheat fields, keeping in mind that 0.52 m was measured over a winter wheat field in the study area during the growing season 2002-2003 (Er-Raki et al., 2007), while Allen et al. (1998) propose values between 1 and 1.8 m for wheat fields. For Zr_{max} set to 0.5 m, optimal results in terms of irrigation accuracy are obtained for a difference ($SM_{fc} - SM_{wp}$) ranging from 0.25 to 0.27 m^3m^{-3}, while by setting Zr_{max} to 1.5 m, optimal results are obtained for a difference ($SM_{fc} - SM_{wp}$) ranging from 0.12 to 0.13 m^3m^{-3}. It is found that the optimal SM_{fc} and SM_{wp} values for Zr_{max} equal to 0.5 m and 1.5 m are not realistic for soils present in the study area. Indeed the difference 0.25 - 0.27 m^3m^{-3} (Zr_{max} = 0.5 m) is much larger than that for clayey soils, and the difference of 0.12 - 0.13 m^3m^{-3} (Zr_{max} = 1.5 m) is typical for sandy soils. Therefore, the sensitivity analysis shows that 1 m is a deemed acceptable value for Zr_{max} that allows obtaining both optimal and realistic SM_{fc} and SM_{wp} values for the main soils present in the study area.

Although good accuracies were found using uniform parameters, Fig. 10. Sensitivity analysis results for the soil parameters SM_{fc} and SM_{wp} by setting Zr_{max} set to 1.0 m. The irrigations are estimated by using SM_{fc} ranging between 0.28 and 0.40 m^3m^{-3} and SM_{wp} ranging between 0.10 and 0.24 m^3m^{-3}. The statistical parameter R (top) and RMSE (bottom) for actual irrigation accumulated over 15 days are estimated by using FAO-$2Kc_{Ks=1}$ (left) and FAO-$2Kc_{Landsat}$ (right) models. The red square indicates the SM_{fc} and SM_{wp} used in the approach.
indicates that the performance can still be improved if optimal values are used by properly adjusting them to the actual soil texture of the crop field.

5 **Conclusion**

A new approach to estimate the field-scale irrigation amounts and timing along the agricultural season is developed by integrating the Landsat optical and thermal data into a crop water balance (FAO-based) model. The main idea behind the approach is first to determine the irrigation date and then to estimate the irrigation amount as the difference between the RZSM estimated on the irrigation date and that estimated on the day before. In order to integrate the Landsat data into a crop water balance model and then to retrieve the irrigation at field scale, four general procedures are implemented: i) partitioning the Landsat LST to derive the crop water stress coefficient Ks, ii) estimating the daily RZSM from the integration of Landsat-derived Ks into a crop water balance model, iii) retrieving irrigation at the Landsat pixel scale and iv) aggregating pixel-scale irrigation estimates at the crop field scale. The approach is assessed over three agricultural areas during four seasons and validated specifically on five winter wheat fields under different irrigation techniques (drip, flood and no-irrigation). The approach is validated in terms of irrigation estimates as well as daily RZSM and ET as intermediate variables linked to the crop water balance model. The approach is compared against the classical approach FAO-2Kc that simulates irrigations to avoid stressed conditions (FAO-$2Kc_{Ks=1}$) and the FAO-2Kc forced by actual irrigations (FAO-$2Kc_{Iobs}$).

The results depict that the proposed approach estimates accurately the total irrigation amounts over all the fields and seasons with a RMSE equal to 44 mm and an R of 0.95. To assess the performance of the irrigation retrieval method at different time scales along the seasons, the daily irrigations are cumulated over overlapping periods of 1 to 90 days (3 months). This analysis shows that acceptable errors are obtained for irrigations cumulated over 15 days and the performance is gradually improved by increasing the accumulation period. This period is closely linked to the revisit time of Landsat data that is 16 days or 8 day when combining Landsat-7 and Landsat-8 data, and often longer in cloudy conditions.

Although the approach does not allow obtaining good performances at daily to weekly scale in terms of irrigation amounts and timing, the daily RZSM and ET simulated from the retrieved irrigations are estimated accurately and are very close to those estimated from actual irrigations (FAO-2Kc$_{Iobs}$). Based on these results, we can conclude that:

i) The approach obtains acceptable errors in irrigation amount and timing in order to simulate the dynamic of water budget components along the season at daily and crop field scale.

ii) The formulation of generic coefficients Kcb and Ke, which are derived analytically from the link between the FAO-2Kc and the image-based model (SSEBop) formalisms allows its implementation to estimate ET accurately at field scale over extended areas by using satellite data. Hence, the Kcb and Ke allow generic implementations avoiding calibration, which usually needs in situ data that are rarely available over extended areas.

This new approach demonstrates the utility of optical and thermal data for estimating the irrigation and then for retrieving the water budget components of crops. However, significant improvements can be expected if the revisit time is reduced with a similar or even improved spatial resolution. In this vein, the advent of the TRISHNA mission at high spatio-temporal resolution in the thermal infrared (Lagouarde and Bhattacharya, 2018), will lead to substantial improvements in the estimation of irrigation at daily to weekly scale. Such an improvement will come not only from a shorter revisit cycles (~3 days), but also from a higher spatial resolution (~50 m), being more suitable for monitoring water consumption at crop field scale. Additionally, some improvements are foreseen to better estimate irrigation timing and the soil coefficients. Better constraining the topsoil layer (soil moisture) would improve the estimation of Kr and Ke coefficients. This issue will be addressed in future studies by integrating the surface soil moisture through a soil evaporative efficiency model (Merlin et al., 2016), which can be derived from active C-band Sentinel-1 data (Amazirh et al., 2018).

Acknowledgement

This study was supported by the European Commission Horizon 2020 Programme for Research and Innovation (H2020) in the context of the Marie Sklodowska-Curie Research and Innovation Staff Exchange (RISE) action (REC project, grant agreement no: 645642 followed by ACCWA project, grant agreement no: 823965). L. Olivera-Guerra acknowledges the support from CONICYT-Chile through the PhD fellowship “BecasChile de Doctorado en el Extranjero” (grant agreement no: 4721/2016).

Appendix A

A.1 Rooting depth Zr

Zr varies according to the vegetation cover between a minimum value (Zr_{min} set to 0.1 m) and a maximum value (Zr_{max} set to 1 m at fv = 1) and is expressed as:

$$Zr_t = Zr_{min} + fv_t(Zr_{max} - Zr_{min}) \tag{A.1}$$

where fv_t is the daily fv interpolated from the Landsat fv estimates. Note that once Zr_t reaches its maximum value at the maximum fv_t it is maintained constant until the end of the season.

A.2 Uncertainty in Landsat-derived RZSM

The Landsat-derived $RZSM_{Landsat,j}$ at date j in the Eq. (5) can be expressed as:

$$RZSM_{Landsat,j} = SM_{wp} + Ks_{Landsat,j}(1-p)\left(SM_{fc} - SM_{wp}\right) \tag{A.2}$$

With p being the tolerance of crop to water stress as a fraction of the total available water. The uncertainty in $RZSM_{Landsat,j}$ is estimated from the propagation of uncertainty method, which takes into account a relative error of every independent variable in the Eq. (A.2) through its partial derivatives. We consider an error of 10% ($\varepsilon = 0.1$) for every variable and therefore the uncertainty in $RZSM_{Landsat,j}$ can be analytically written as:

$$e_{RZSM_{Landsat},j} = \left\{SM_{wp} + Ks_{Landsat,j}(2-3p)\left(SM_{fc} - SM_{wp}\right)\right\}\varepsilon \tag{A.3}$$

A.3 Landsat-derived Kcb and Ke

In order to take advantage of satellite data for generic implementations, we link the FAO-2Kc formalism with a contextual model to estimate the main parameters Kcb and Ke. As it is expressed in Eq. (A.4), the dual crop coefficient FAO-2Kc ET is made equal to the single source Operational Simplified Surface Energy Balance (SSEBop, Senay et al., 2013) formalism in order to derive the coefficients required in FAO-2Kc.

$$(Ks \cdot Kcb + Ke)ET_0 = ET = EF \cdot Kc_{max} \cdot ET_0 \tag{A.4}$$

where ET0 is the reference evapotranspiration, EF the evaporative fraction (defined as the ratio of ET to available energy) and Kc_{max} the coefficient to scale the ET_0 down to the maximum ET reached by a crop. On the left-hand side of the equation, FAO-2Kc model estimates the ET from a crop basal coefficient (Kcb) and an evaporation coefficient (Ke), respectively, weighted by ET_0. The transpiration component (Kcb ET_0) is controlled by the crop stress coefficient (Ks) and the evaporation (Ke ET_0) is controlled by the evaporation reduction coefficient (Kr). On the right-hand side of the equation, SSEBop uses Kc_{max} modulated by EF as a single crop coefficient containing the transpiration and evaporation coefficients. EF can be estimated as:

$$EF = \frac{LST_{max} - LST}{LST_{max} - LST_{min}} \tag{A.5}$$

where LST_{min} and LST_{max} are the minimum and maximum LST representing the wet/unstressed and dry/stressed conditions (see *Fig. 3*), respectively, as has been used in several contextual methods (e.g. Roerink et al., 2000; Merlin et al., 2013; Merlin et al., 2014). Given that Kr, Ks and EF are estimated from thermal and fv data in our study, every term used in (A.5) is partitioned into its vegetation and soil components in such a way that Ke and Kcb formulations can be analytically derived from the equality in Eq. (A.4), as it is described below.

By partitioning every term in A.5, EF can be expressed as:

$$EF = \frac{[fvTv_{max} + (1-fv)Ts_{max}] - [fvTv + (1-fv)Ts]}{[fvTv_{max} + (1-fv)Ts_{max}] - [fvTv_{min} + (1-fv)Ts_{min}]} \tag{A.6}$$

By introducing the Landsat-derived Ks and Kr into A.6, SSEBop ET in Eq. (A.4) can be rewritten as:

$$ET = \left[\frac{fv(Tv_{max} - Tv_{min})Ks + (1-fv)(Ts_{max} - Ts_{min})Kr}{fv(Tv_{max} - Tv_{min}) + (1-fv)(Ts_{max} - Ts_{min})} \cdot Kc_{max}\right] \cdot ET_0 \tag{A.7}$$

For clarity we set $\Delta Tv = Tv_{max} - Tv_{min}$ and $\Delta Ts = Ts_{max} - Ts_{min}$ in A.7. By re-arranging, two terms related to the vegetation and soil components are highlighted:

$$ET = \left[\frac{fv(\Delta Tv)Ks}{fv(\Delta Tv) + (1 - fv)(\Delta Ts)} Kc_{max} + \frac{(1 - fv)(\Delta Ts)Kr}{fv(\Delta Tv) + (1 - fv)(\Delta Ts)} Kc_{max}\right] \cdot ET_0 \tag{A.8}$$

where the first term in parentheses can be considered as the transpiration coefficient (Ks Kcb) and the second as Ke, as they are depicted in the FAO-2Kc formalism (Eq. (A.4)). To simplify Kcb and Ke formulations, ΔTv is assumed close to ΔTs in A.8 as in previous works (Olivera-Guerra et al., 2018; Stefan et al., 2015). Hence the following simple expressions are derived:

$$Kcb = fvKc_{max} \tag{A.9}$$

$$Ke = (1 - fv)KrKc_{max} \tag{A.10}$$

where Kcb depends on *fv* while Ke depends on the soil fraction (*1 – fv*) weighted by Kr and Kc_{max}. These expressions are consistent with the FAO-2kc calibrated with vegetation index proposed in the literature (e.g. Er-Raki et al., 2010; Kullberg et al., 2016; Simonneaux et al., 2008). In this study, Kc_{max} is set to 1.2 as a typical recommended value (Allen et al., 2011; Senay et al., 2013; Senay et al., 2016).

References

Ait Hssaine, B., Merlin, O., Rafi, Z., Ezzahar, J., Jarlan, L., Khabba, S., Er-Raki, S., 2018. Calibrating an evapotranspiration model using radiometric surface temperature, vegetation cover fraction and near-surface soil moisture data. Agric. For. Meteorol. 256–257, 104–115. https://doi.org/10.1016/J.AGRFORMET.2018.02.033

Allen, R.G., Pereira, L.S., Howell, T. a., Jensen, M.E., 2011. Evapotranspiration information reporting: I. Factors governing measurement accuracy. Agric. Water Manag. 98, 899–920. https://doi.org/10.1016/j.agwat.2010.12.015

Allen, R.G., Pereira, L.S., Raes, D., Smith., M., 1998. Crop evapotranspiration - Guidlines for computing crop water requirements. Irrig. Drainage. Pap. 56, Food Agriciculture. Organ. United Nations, Rome, Italy.

Amazirh, A., Er-Raki, S., Chehbouni, A., Rivalland, V., Diarra, A., Khabba, S., Ezzahar, J., Merlin, O., 2017. Modified Penman–Monteith equation for monitoring evapotranspiration of wheat crop: Relationship between the surface resistance and remotely sensed stress index. Biosyst. Eng. 164, 68–84. https://doi.org/10.1016/j.biosystemseng.2017.09.015

Amazirh, A., Merlin, O., Er-Raki, S., 2019. Including Sentinel-1 radar data to improve the disaggregation of MODIS land surface temperature data. ISPRS J. Photogramm. Remote Sens. 150, 11–26. https://doi.org/10.1016/j.isprsjprs.2019.02.004

Amazirh, A., Merlin, O., Er-Raki, S., Gao, Q., Rivalland, V., Malbeteau, Y., Khabba, S., Escorihuela, M.J., 2018. Retrieving surface soil moisture at high spatio-temporal resolution from a synergy between Sentinel-1 radar and Landsat thermal data: a study case over bare soil. Remote Sens. Environ. 211, 321–337. https://doi.org/10.1016/j.rse.2018.04.013

Anderson, M.C., Allen, R.G., Morse, A., Kustas, W.P., 2012. Use of Landsat thermal imagery in monitoring evapotranspiration and managing water resources. Remote Sens.

Environ. 122, 50–65. https://doi.org/10.1016/j.rse.2011.08.025

Baldridge, A.M., Hook, S.J., Grove, C.I., Rivera, G., 2009. The ASTER spectral library version 2.0. Remote Sens. Environ. 113, 711–715. https://doi.org/10.1016/j.rse.2008.11.007

Bastiaanssen, W.G.M., Allen, R.G., Droogers, P., D'Urso, G., Steduto, P., 2007. Twenty-five years modeling irrigated and drained soils: State of the art. Agric. Water Manag. 92, 111–125. https://doi.org/10.1016/j.agwat.2007.05.013

Battude, M., Al, A., Brut, A., Tallec, T., Huc, M., Cros, J., Weber, J., Lhuissier, L., Simonneaux, V., 2017. Modeling water needs and total irrigation depths of maize crop in the south west of France using high spatial and temporal resolution satellite imagery. Agric. Water Manag. 189, 123–136. https://doi.org/10.1016/j.agwat.2017.04.018

Boulet, G., Chehbouni, A., Gentine, P., Duchemin, B., Ezzahar, J., Hadria, R., 2007. Monitoring water stress using time series of observed to unstressed surface temperature difference. Agric. For. Meteorol. 146, 159–172. https://doi.org/10.1016/j.agrformet.2007.05.012

Brocca, L., Ciabatta, L., Massari, C., Camici, S., Tarpanelli, A., 2017. Soil moisture for hydrological applications: Open questions and new opportunities. Water (Switzerland) 9. https://doi.org/10.3390/w9020140

Brocca, L., Tarpanelli, A., Filippucci, P., Dorigo, W., Zaussinger, F., Gruber, A., Fernández-Prieto, D., 2018. How much water is used for irrigation? A new approach exploiting coarse resolution satellite soil moisture products. Int. J. Appl. Earth Obs. Geoinf. 73, 752–766. https://doi.org/10.1016/j.jag.2018.08.023

Chehbouni, A., Escadafal, R., Duchemin, B., Boulet, G., Simonneaux, V., Dedieu, G., Mougenot, B., Khabba, S., Kharrou, H., Maisongrande, P., Merlin, O., Chaponnière, A., Ezzahar, J., Er-Raki, S., Hoedjes, J., Hadria, R., Abourida, A., Cheggour, A., Raibi, F., Boudhar, A., Benhadj, I., Hanich, L., Benkaddour, A., Guemouria, N., Chehbouni, A.H., Lahrouni, A., Olioso, A., Jacob, F., Williams, D.G., Sobrino, J.A., 2008. An integrated modelling and remote sensing approach for hydrological study in arid and semi-arid regions: The SUDMED programme. Int. J. Remote Sens. 29, 5161–5181. https://doi.org/10.1080/01431160802036417

Chen, Y., Lu, D., Luo, L., Pokhrel, Y., Deb, K., Huang, J., Ran, Y., 2018. Detecting irrigation extent, frequency, and timing in a heterogeneous arid agricultural region using MODIS time series, Landsat imagery, and ancillary data. Remote Sens. Environ. 204, 197–211. https://doi.org/10.1016/j.rse.2017.10.030

Corbari, C., Ceppi, A., Telesca, V., Mancini, M., 2019. Smart irrigation forecast using satellite LANDSAT data and meteo- hydrological modeling. Agric. Water Manag. 212, 283–294. https://doi.org/10.1016/j.agwat.2018.09.005

Droogers, P., Immerzeel, W.W., Lorite, I.J., 2010. Estimating actual irrigation application by remotely sensed evapotranspiration observations. Agric. Water Manag. 97, 1351–1359. https://doi.org/10.1016/j.agwat.2010.03.017

Duan, S.B., Li, Z.L., Wang, C., Zhang, S., Tang, B.H., Leng, P., Gao, M.F., 2018. Land-surface temperature retrieval from Landsat 8 single-channel thermal infrared data in combination with NCEP reanalysis data and ASTER GED product. Int. J. Remote Sens. 00, 1–16. https://doi.org/10.1080/01431161.2018.1460513

Duchemin, B., Hadria, R., Erraki, S., Boulet, G., Maisongrande, P., Chehbouni, A., Escadafal, R., Ezzahar, J., Hoedjes, J.C.B., Kharrou, M.H., Khabba, S., Mougenot, B., Olioso, A., Rodriguez, J.-C., Simonneaux, V., 2006. Monitoring wheat phenology and irrigation in Central Morocco: On the use of relationships between evapotranspiration, crops coefficients, leaf area index and remotely-sensed vegetation indices. Agric. Water Manag. 79, 1–27. https://doi.org/10.1016/j.agwat.2005.02.013

Duchemin, B., Maisongrande, P., Boulet, G., Benhadj, I., 2008. A simple algorithm for yield estimates: Evaluation for semi-arid irrigated winter wheat monitored with green leaf area index. Environ. Model. Softw. 23, 876–892. https://doi.org/10.1016/j.envsoft.2007.10.003

Er-Raki, S., Chehbouni, A., Duchemin, B., 2010. Combining satellite remote sensing data with the FAO-56 dual approach for water use mapping in irrigated wheat fields of a semi-arid region. Remote Sens. 2, 375–387. https://doi.org/10.3390/rs2010375

Er-Raki, S., Chehbouni, A., Guemouria, N., Duchemin, B., Ezzahar, J., Hadria, R., 2007. Combining FAO-56 model and ground-based remote sensing to estimate water consumptions of wheat crops in a semi-arid region. Agric. Water Manag. 87, 41–54. https://doi.org/10.1016/j.agwat.2006.02.004

Escorihuela, M.J., Quintana-Seguí, P., 2016. Comparison of remote sensing and simulated soil moisture datasets in Mediterranean landscapes. Remote Sens. Environ. 180, 99–114. https://doi.org/10.1016/j.rse.2016.02.046

Foley, J.A., Ramankutty, N., Brauman, K.A., Cassidy, E.S., Gerber, J.S., Johnston, M., Mueller, N.D., O'Connell, C., Ray, D.K., West, P.C., Balzer, C., Bennett, E.M., Carpenter, S.R., Hill, J., Monfreda, C., Polasky, S., Rockström, J., Sheehan, J., Siebert, S., Tilman, D., Zaks, D.P.M., 2011. Solutions for a cultivated planet. Nature 478, 337–342. https://doi.org/10.1038/nature10452

Garrido, A., Llamas, M.R., Varela-Ortega, C., Novo, P., Rodríguez-Casado, R., Aldaya, M.M., 2010. Water Footprint and Virtual Water Trade in Spain. Policy Implications. Series: Natural Resource Management and Policy, 35. IX, 150. https:///doi.org/10.1007/978-1-4419-5741-2

Giorgi, F., 2006. Climate change hot-spots. Geophys. Res. Lett. 33, 1–4. https://doi.org/10.1029/2006GL025734

Gowda, P.H., Chavez, J.L., Colaizzi, P.D., Evett, S.R., Howell, T.A., Tolk, J.A., 2008. ET mapping for agricultural water management: present status and challenges. Irrig. Sci. 26, 223–237. https://doi.org/10.1007/s00271-007-0088-6

Gutman, G., Ignatov, A., 1998. The derivation of the green vegetation fraction from NOAA/AVHRR. Int. J. Remote Sens. 19, 1533–1543. https://doi.org/https://doi.org/10.1080/014311698215333

Hain, C.R., Mecikalski, J.R., Anderson, M.C., 2009. Retrieval of an Available Water-Based Soil Moisture Proxy from Thermal Infrared Remote Sensing. Part I: Methodology and Validation. J. Hydrometeorol. 10, 665–683. https://doi.org/10.1175/2008JHM1024.1

IPCC, 2013. Climate Change 2013: The Physical Science Basis. Contribution of Working Group I to the Fifth Assessment Report of the Intergovernmental Panel on Climate Change. Ed. Stocker, T.F., et al.. Cambridge University Press, Cambridge, United Kingdom and New York, NY, USA, 1535.0

Jalilvand, E., Tajrishy, M., Ghazi Zadeh Hashemi, S.A., Brocca, L., 2019. Quantification of irrigation water using remote sensing of soil moisture in a semi-arid region. Remote Sens. Environ. 231, 111226. https://doi.org/10.1016/j.rse.2019.111226

Jiang, L., Islam, S., 2003. An intercomparison of regional latent heat flux estimation using remote sensing data. Int. J. Remote Sens. 24, 2221–2236. https://doi.org/10.1080/01431160210154821

Jiménez-Muñoz, J.C., Sobrino, J.A., Skokovi´, D., Mattar, C., Cristóbal, J., 2014. Land surface temperature retrieval methods from Landsat-8 thermal infrared sensor data. Geosci. Remote Sens. Lett. IEEE 11, 1840–1843. https://doi.org/10.1109/LGRS.2014.2312032

Jiménez-Munoz, J.C., Sobrino, J.A., Sòria, G., Cristobal, J., Pons, X., Ninyerola, M., 2009.

Revision of the single-channel algorithm for land surface temperature retrieval from landsat thermal-infrared data. IEEE Trans. Geosci. Remote Sens. 47, 339–349. https://doi.org/10.1109/TGRS.2008.2007125

Kalma, J.D., McVicar, T.R., McCabe, M.F., 2008. Estimating land surface evaporation: A review of methods using remotely sensed surface temperature data. Surv. Geophys. 29, 421–469. https://doi.org/10.1007/s10712-008-9037-z

Kullberg, E.G., DeJonge, K.C., Chávez, J.L., 2016. Evaluation of thermal remote sensing indices to estimate crop evapotranspiration coefficients. Agric. Water Manag. 179, 64–73. https://doi.org/10.1016/j.agwat.2016.07.007

Kumar, S. V., Peters-Lidard, C.D., Santanello, J.A., Reichle, R.H., Draper, C.S., Koster, R.D., Nearing, G., Jasinski, M.F., 2015. Evaluating the utility of satellite soil moisture retrievals over irrigated areas and the ability of land data assimilation methods to correct for unmodeled processes. Hydrol. Earth Syst. Sci. 19, 4463–4478. https://doi.org/10.5194/hess-19-4463-2015

Lagouarde, J., Bhattacharya, B.K., 2018. TRISHNA : a new high spatio-temporal resolution Indian-French mission in the thermal infrared, in: Remote Sensing and Hydrology Symposium (ICRS-IAHS).

Lawston, P.M., Santanello, J.A., Kumar, S. V., 2017. Irrigation Signals Detected From SMAP Soil Moisture Retrievals. Geophys. Res. Lett. 44, 11,860-11,867. https://doi.org/10.1002/2017GL075733

Le Page, M., Toumi, J., Khabba, S., Hagolle, O., Tavernier, A., Hakim Kharrou, M., Er-Raki, S., Huc, M., Kasbani, M., Moutamanni, A. El, Yousfi, M., Jarlan, L., 2014. A life-size and near real-time test of irrigation scheduling with a sentinel-2 like time series (SPOT4-Take5) in Morocco. Remote Sens. 6, 11182–11203. https://doi.org/10.3390/rs61111182

Li, Z.-L., Tang, R., Wan, Z., Bi, Y., Zhou, C., Tang, B., Yan, G., Zhang, X., 2009. A review of current methodologies for regional evapotranspiration estimation from remotely sensed data. Sensors (Basel). 9, 3801–53. https://doi.org/10.3390/s90503801

Long, D., Singh, V.P., 2012. A Two-source Trapezoid Model for Evapotranspiration (TTME) from satellite imagery. Remote Sens. Environ. 121, 370–388. https://doi.org/10.1016/j.rse.2012.02.015

Malakar, N.K., Hulley, G.C., Hook, S.J., Laraby, K., Cook, M., Schott, J.R., 2018. An Operational Land Surface Temperature Product for Landsat Thermal Data: Methodology and Validation. IEEE Trans. Geosci. Remote Sens. 5717–5735. https://doi.org/10.1109/TGRS.2018.2824828

Malbéteau, Y., Merlin, O., Balsamo, G., Er-Raki, S., Khabba, S., Walker, J.P., Jarlan, L., 2018. Toward a Surface Soil Moisture Product at High Spatiotemporal Resolution: Temporally Interpolated, Spatially Disaggregated SMOS Data. J. Hydrometeorol. 19, 183–200. https://doi.org/10.1175/jhm-d-16-0280.1

Merlin, O., 2013. An original interpretation of the wet edge of the surface temperature-albedo space to estimate crop evapotranspiration (SEB-1S), and its validation over an irrigated area in northwestern Mexico. Hydrol. Earth Syst. Sci. 17, 3623–3637. https://doi.org/10.5194/hess-17-3623-2013

Merlin, O., Al Bitar, A., Rivalland, V., Béziat, P., Ceschia, E., Dedieu, G., 2011. An analytical model of evaporation efficiency for unsaturated soil surfaces with an arbitrary thickness. J. Appl. Meteorol. Climatol. 50, 457–471.

Merlin, O., Chirouze, J., Olioso, A., Jarlan, L., Chehbouni, G., Boulet, G., 2014. An image-based four-source surface energy balance model to estimate crop evapotranspiration from solar reflectance/thermal emission data (SEB-4S). Agric. For. Meteorol. 184, 188–203. https://doi.org/10.1016/j.agrformet.2013.10.002

Merlin, O., Escorihuela, M.J., Mayoral, M.A., Hagolle, O., Al Bitar, A., Kerr, Y., 2013. Self-calibrated evaporation-based disaggregation of SMOS soil moisture: An evaluation study at 3km and 100m resolution in Catalunya, Spain. Remote Sens. Environ. 130, 25–38. https://doi.org/10.1016/j.rse.2012.11.008

Merlin, O., Olivera-guerra, L., Aït, B., Amazirh, A., Ra, Z., Ezzahar, J., Gentine, P., Khabba, S., Gascoin, S., Er-raki, S., 2018. A phenomenological model of soil evaporative efficiency using surface soil moisture and temperature data. Agric. For. Meteorol. 256–257, 501–515. https://doi.org/10.1016/j.agrformet.2018.04.010

Merlin, O., Rüdiger, C., Bitar, A. Al, Richaume, P., Walker, J.P., Kerr, Y.H., 2012. Disaggregation of SMOS Soil Moisture in Southeastern Australia. IEEE Trans. Geosci. Remote Sens. 50, 1556–1571.

Merlin, O., Stefan, V.G., Amazirh, A., Chanzy, A., Ceschia, E., Tallec, T., Beringer, J., Gentine, P., Er-Raki, S., Bircher, S., Khabba, S., 2016. Modeling soil evaporation efficiency in a range of soil and atmospheric conditions: A downward approach based on multi-site data. Water Resour. Res. 52, 3663–3684. https://doi.org/10.1002/2015WR018233.

Molero, B., Merlin, O., Malbéteau, Y., Al Bitar, A., Cabot, F., Stefan, V., Kerr, Y., Bacon, S., Cosh, M.H., Bindlish, R., Jackson, T.J., 2016. SMOS disaggregated soil moisture product at 1 km resolution: Processor overview and first validation results. Remote Sens. Environ. 180, 361–376. https://doi.org/10.1016/j.rse.2016.02.045

Moran, M.S., Clarke, T.R., Inoue, Y., Vidal, A., 1994. Estimating crop water deficit using the relation between surface-air temperature and spectral vegetation index. Remote Sens. Environ. 49, 246–263. https://doi.org/10.1016/0034-4257(94)90020-5

Norman, J.M., Kustas, W.P., Humes, K.S., 1995. A two-source approach for estimating soil and vegetation energy fluxes in observations of directional radiometric surface temperature. Agric. For. Meteorol. 77, 263–293. https://doi.org/10.1016/0168-

1923(95)02265-Y

Ogawa, K., Schmugge, T., 2004. Mapping Surface Broadband Emissivity of the Sahara Desert Using ASTER and MODIS Data. Earth Interact. 8, 1–14. https://doi.org/10.1175/1087-3562(2004)008<0001:MSBEOT>2.0.CO;2

Olivera-Guerra, L., Merlin, O., Er-raki, S., Khabba, S., Escorihuela, M.-J., 2018. Estimating the water budget components of irrigated crops: Combining the FAO-56 dual crop coefficient with surface temperature and vegetation index data. Agric. Water Manag. 208, 120–131. https://doi.org/10.1016/j.agwat.2018.06.014

Peng, J., Loew, A., Merlin, O., Verhoest, N.E.C., 2017. A review of spatial downscaling of satellite remotely sensed soil moisture. Rev. Geophys. 55, 341–366. https://doi.org/10.1002/2016RG000543

Rafi, Z., Merlin, O., Le Dantec, V., Khabba, S., Mordelet, P., Er-raki, S., Amazirh, A., Olivera-guerra, L., Ait Hssaine, B., 2019. Partitioning evapotranspiration of a drip-irrigated wheat crop : Inter- comparing eddy covariance-, sap flow-, lysimeter- and FAO-based methods. Agric. For. Meteorol. 265, 310–326. https://doi.org/10.1016/j.agrformet.2018.11.031

Roerink, G.J., Su, Z., Menenti, M., 2000. S-SEBI: A simple remote sensing algorithm to estimate the surface energy balance. Phys. Chem. Earth, Part B Hydrol. Ocean. Atmos. 25, 147–157. https://doi.org/10.1016/S1464-1909(99)00128-8

Romaguera, M., Krol, M.S., Salama, M.S., Su, Z., Hoekstra, A.Y., 2014. Application of a remote sensing method for estimating monthly blue water evapotranspiration in irrigated agriculture. Remote Sens. 6, 10033–10050. https://doi.org/10.3390/rs61010033

Sandholt, I., Rasmussen, K., Andersen, J., 2002. A simple interpretation of the surface temperature/vegetation index space for assessment of surface moisture status. Remote Sens. Environ. 79, 213–224. https://doi.org/10.1016/S0034-

4257(01)00274-7

Senay, G.B., Bohms, S., Singh, R.K., Gowda, P.H., Velpuri, N.M., Alemu, H., Verdin, J.P., 2013. Operational Evapotranspiration Mapping Using Remote Sensing and Weather Datasets: A New Parameterization for the SSEB Approach. JAWRA J. Am. Water Resour. Assoc. 49, 577–591. https://doi.org/10.1111/jawr.12057

Senay, G.B., Friedrichs, M., Singh, R.K., Velpuri, N.M., 2016. Evaluating Landsat 8 evapotranspiration for water use mapping in the Colorado River Basin. Remote Sens. Environ. 185, 171–185. https://doi.org/10.1016/j.rse.2015.12.043

Simonneaux, V., Duchemin, B., Helson, D., Er-Raki, S., Olioso, A., Chehbouni, A.G., 2008. The use of high-resolution image time series for crop classification and evapotranspiration estimate over an irrigated area in central Morocco. Int. J. Remote Sens. 29, 95–116. https://doi.org/10.1080/01431160701250390

Sobrino, J.A., Jiménez-muñoz, J.C., Sòria, G., Romaguera, M., Guanter, L., Moreno, J., Plaza, A., Martínez, P., 2008. Land Surface Emissivity Retrieval From Different VNIR and TIR Sensors. IEEE Trans. Geosci. Remote Sens. 46, 316–327.

Stefan, V.G., Merlin, O., Er-Raki, S., Escorihuela, M.J., Khabba, S., 2015. Consistency between In Situ, model-derived and high-resolution-image-based soil temperature endmembers: Towards a robust data-based model for multi-resolution monitoring of crop evapotranspiration. Remote Sens. 7, 10444–10479. https://doi.org/10.3390/rs70810444

van Eekelen, M.W., Bastiaanssen, W.G.M., Jarmain, C., Jackson, B., Ferreira, F., 2015. A novel approach to estimate direct and indirect water withdrawals from satellite measurements : A case study from the Incomati basin. Agric. Ecosyst. Environ. 200, 126–142. https://doi.org/10.1016/j.agee.2014.10.023

Werner, B.; Collins, R. et. al., 2012. Towards efficient use of water resources in Europe.

EEA Report | No 1/2012, European Environment Agency, Copenhagen. https://doi.org/10.2800/95096

Wosten, J.H.M., Lilly, A., Nemes, A., Le Bas, C., 1999. Development and use of a database of hydraulic properties of European soils. Geoderma 90, 169–218.

Zhang, X., Qiu, J., Leng, G., Yang, Y., Gao, Q., 2018. The Potential Utility of Satellite Soil Moisture Retrievals for Detecting Irrigation Patterns in China. Water 10, 1–19. https://doi.org/10.3390/w10111505

Tables

Table 1. Main characteristics of experimental winter wheat fields by agricultural area.

Area	Site name	Crop field area	Soil texture (%clay, %sand	Irrigation system	Monitoring period (mm/yyyy)	Total Irrigation applied	# events	Mean irrigation (mm)
Chichaoua	EC1	~1.5 ha	Clay loam (32.5%, 37.5%)	Drip-irrigated	11/2016-5/2017	374	25	15.0 (±5.6)
					11/2017-5/2018	327	26	12.6 (±11.2)
	EC2	~1.5 ha			11/2016-5/2017	504	37	13.6 (±5.7)
					11/2017-5/2018	528	38	13.9 (±11.4)
R3	4ha	4 ha	Clay (47%, 18%)	Flood-irrigated	12/2015-5/2016	448	7	64.0 (-)
	2ha[1]	2 ha		Drip-irrigated	12/2015-5/2016	268	8	29.3 (±7.6)
Sidi Rahal	Bour	~1 ha	Loam (18%, 41%)	Rainfed	10/2014-5/2015	0	0	0
					10/2015-5/2016	0	0	0
					10/2016-5/2017	0	0	0
					10/2017-5/2018	0	0	0

1. R3-2ha field is actually irrigated by drip system with amounts and quantities according to a flood irrigation system. Thus, R3-2ha is considered as flood-irrigated site.

Table 2. Correlation coefficient (R) and root mean square error (RMSE) between observed and simulated RZSM from FAO-2Kc forced by observed irrigation (FAO-2Kc$_{Iobs}$), irrigation triggered avoiding stress (FAO-2Kc$_{Ks=1}$) and irrigation retrieved from the proposed methodology (FAO-2Kc$_{Landsat}$).

Area	Site-season	R (-)			RMSE (m^3/m^3)		
		FAO-2Kc$_{Iobs}$	FAO-2Kc$_{Ks=1}$	FAO-2Kc$_{Landsat}$	FAO-2Kc$_{Iobs}$	FAO-2Kc$_{Ks=1}$	FAO-2Kc$_{Landsat}$
R3	R3-4ha	0.95	0.26	0.73	0.02	0.06	0.04
	R3-2ha	0.90	0.54	0.68	0.03	0.06	0.05
Chichaoua	EC1-2017	0.91	0.19	0.59	0.06	0.08	0.06
	EC2-2017	0.39	0.09	0.25	0.08	0.06	0.06
	EC1-2018	0.87	0.29	0.84	0.03	0.06	0.03
	EC2-2018	0.58	0.25	0.52	0.04	0.03	0.03
Sidi Rahal	Bour-2015	0.64	0.16	0.70	0.05	0.08	0.06
	Bour-2016	0.77	0.22	0.72	0.03	0.09	0.03
	Bour-2017	0.72	0.18	0.72	0.03	0.07	0.03
	Bour-2018	0.76	0.28	0.81	0.03	0.07	0.03
	All	0.75	0.25	0.66	0.04	0.07	0.04

Table 3. Correlation coefficient (R) and root mean square error (RMSE) between observed and simulated ET from FAO-2Kc forced by observed irrigation (FAO-2Kc$_{Iobs}$), irrigation triggered avoiding stress (FAO-2Kc$_{Ks=1}$) and irrigation retrieved from the proposed methodology (FAO-2Kc$_{Landsat}$).

Area	R (-)	RMSE (mm/d)

	Site-season	FAO-2Kc$_{Iobs}$	FAO-2Kc$_{Ks=1}$	FAO-2Kc$_{Landsat}$	FAO-2Kc$_{Iobs}$	FAO-2Kc$_{Ks=1}$	FAO-2Kc$_{Landsat}$
R3	Grav-2016	0.95	0.90	0.94	0.87	0.98	0.88
	Gag-2016	0.92	0.77	0.85	0.68	0.97	0.78
Chichaoua	EC1-2017	0.87	0.79	0.75	0.89	0.88	0.94
	EC2-2017	0.91	0.90	0.89	0.85	1.00	1.06
	EC1-2018	0.64	0.83	0.74	1.37	0.76	1.22
	EC2-2018	0.73	0.87	0.91	1.12	0.77	0.65
Sidi Rahal	Bour-2015	0.81	0.41	0.84	0.63	1.50	0.75
	Bour-2016	0.69	0.25	0.60	0.66	3.03	0.71
	Bour-2017	0.74	0.12	0.74	0.53	1.50	0.53
	Bour-2017	0.86	0.05	0.80	0.61	2.10	0.80
	All	0.81	0.59	0.81	0.82	1.35	0.83

Figures

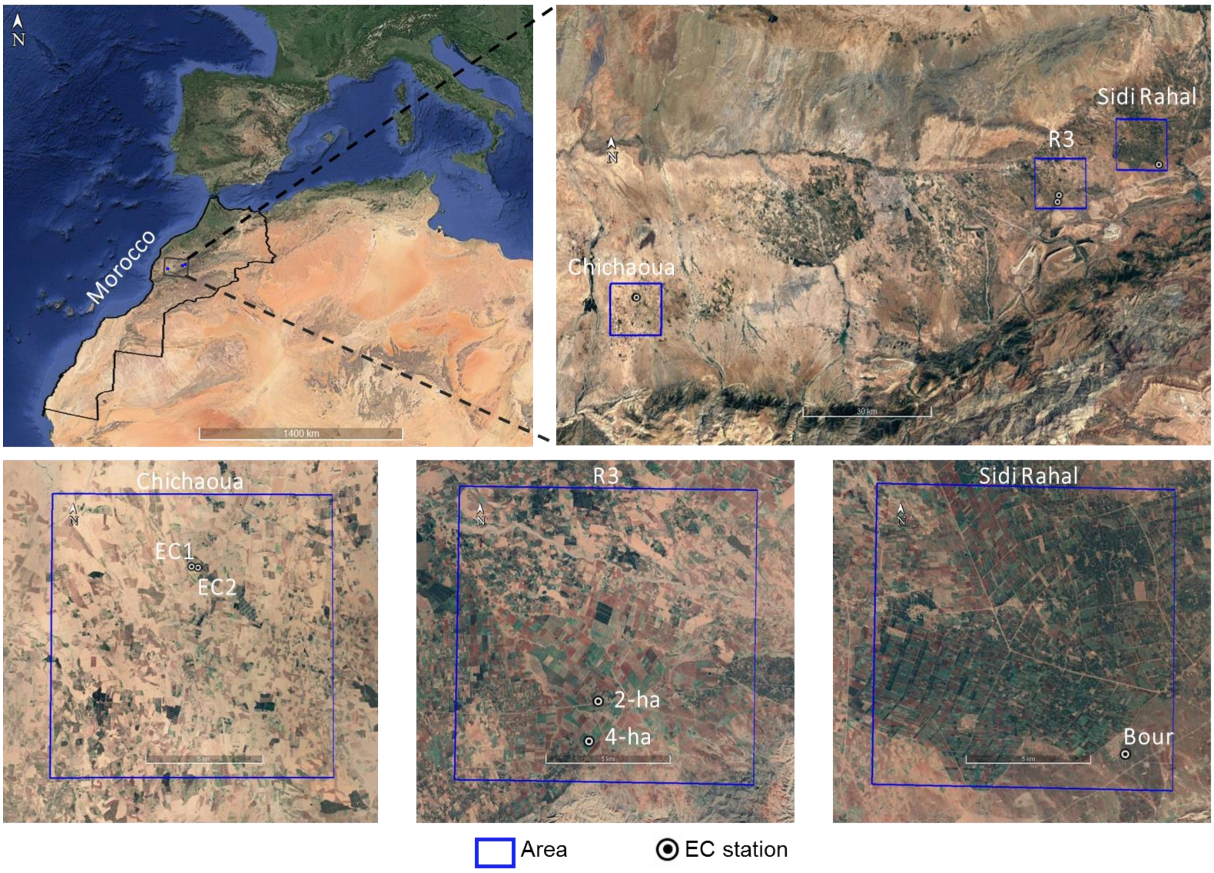

Fig. *1*. Study areas and field crops where the developed approach is evaluated.

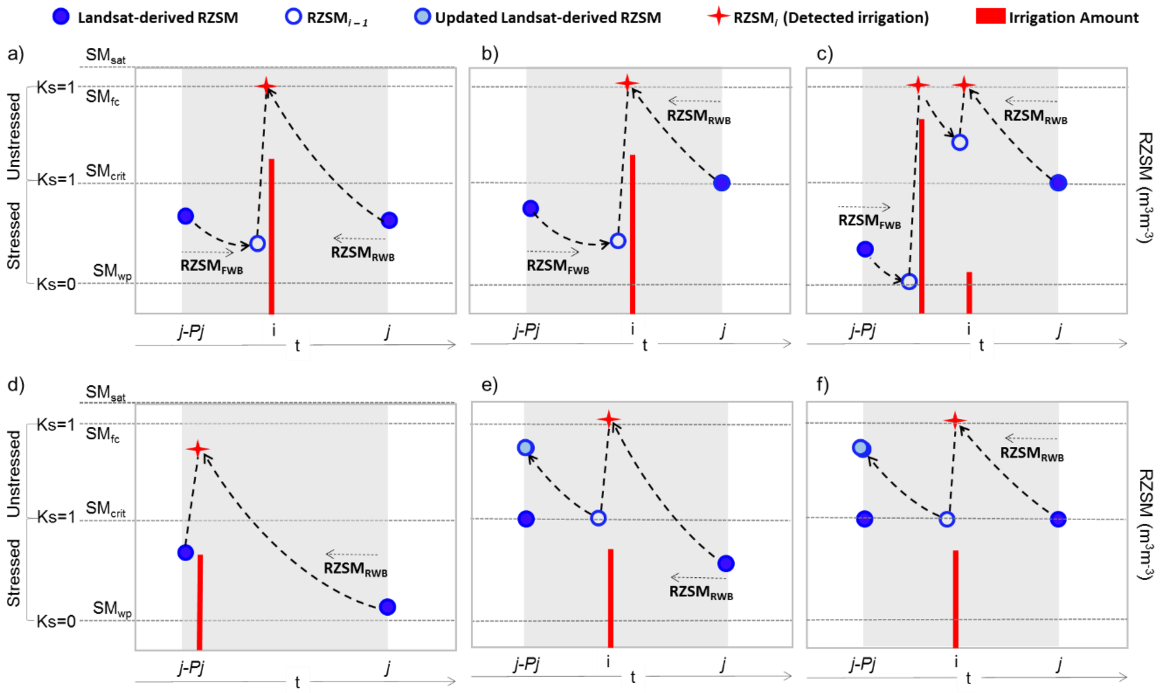

Fig. *2*. Schematic representation of pixel-scale irrigation retrieval between two successive Landsat overpass dates in four different cases: stressed-stressed (a), stressed-unstressed (b), unstressed-stressed (e) and unstressed-unstressed (f). The specific conditions c) and d) can be found in the stressed-(un)stressed cases (a,b). The RZSM is estimated from the FWB (right dotted arrow) or the RBW (left dotted arrow) initialized by the $RZSM_{Landsat}$ at date *j* and *j-Pj*, respectively. An irrigation event is detected when $RZSM_{RWB}$ reaches SM_{fc} and its amount is estimated by the difference between the RZSM retrieved at date *i* and *i-1*.

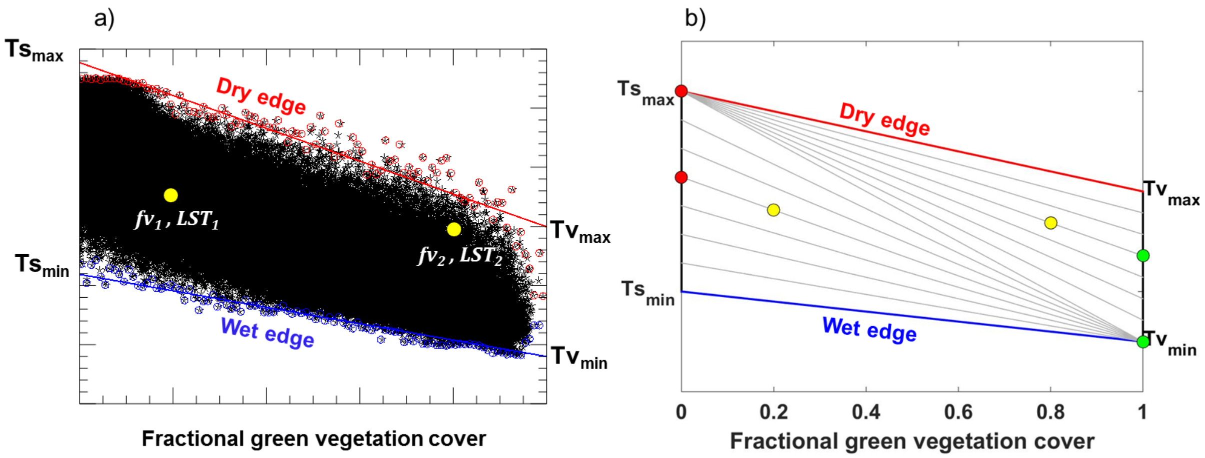

Fig. 3. In a), example of LST-fv feature space constrained by the polygon Ts_{min}-Tv_{min}-Tv_{max}-Ts_{max} from the linear regression of the minimum and maximum LST by fv classes. In b), a conceptual diagram of the LST-fv polygon for partitioning LST for two pixels (*fv,LST*) (yellow points) showing its Ts (red points) and Tv (green points) values corresponding to the TSEB assumptions.

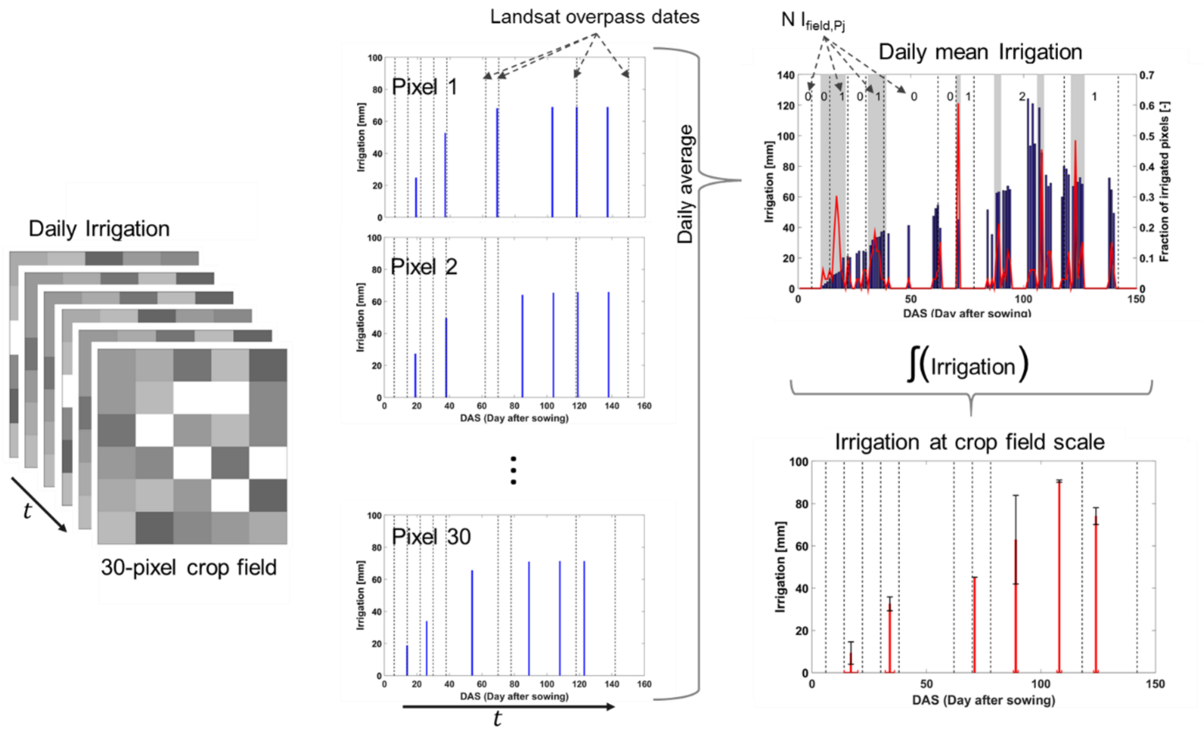

Fig. 4. Schematic diagram presenting the crop field scale irrigation retrieval from pixel-scale irrigation estimates for an example of a 30-pixel crop field. The daily pixel-scale irrigation is represented for every pixel (middle plots), from which are estimated the daily averaged irrigation (blue bar in top right plot) and the fraction of irrigated pixels (red line). Between two successive Landsat overpass dates in top right plot, the daily mean irrigation is integrated in the periods (shaded areas) according to its fractional irrigated pixels. The crop field scale irrigation (red bar in bottom right plot) is obtained by deriving the most probable irrigation date and is provided with its standard deviation for amount (black error bar) and date (red error bar).

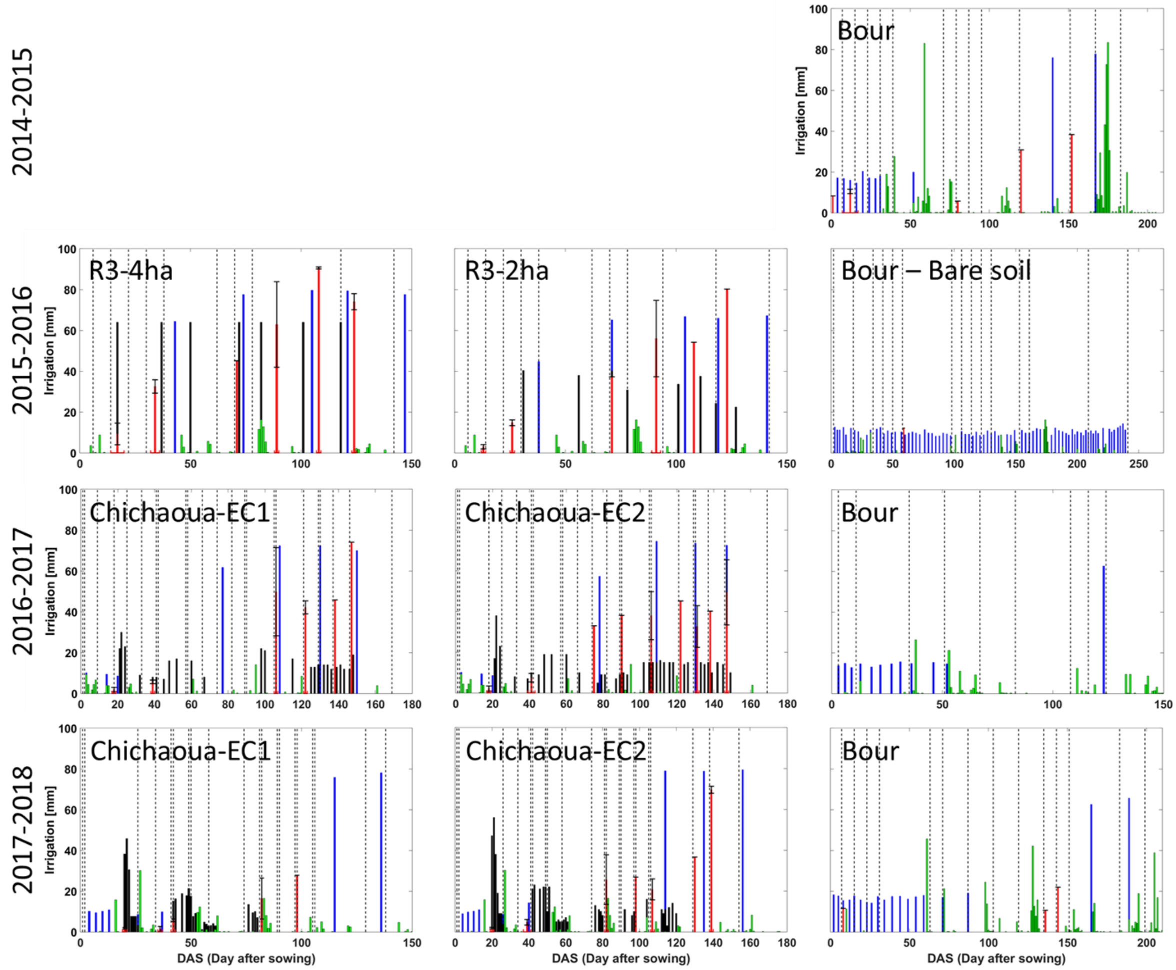

Fig. 5. Comparison between volumes and timing of the observed irrigation (black), irrigation triggered by avoiding stress (blue) and irrigation retrieved from the proposed approach (red) along the season for each site. The horizontal and vertical error bars represent the standard deviation of the retrieved irrigation dates and amounts, respectively. The green bar indicates the precipitation and the vertical dotted lines indicate the Landsat overpass dates.

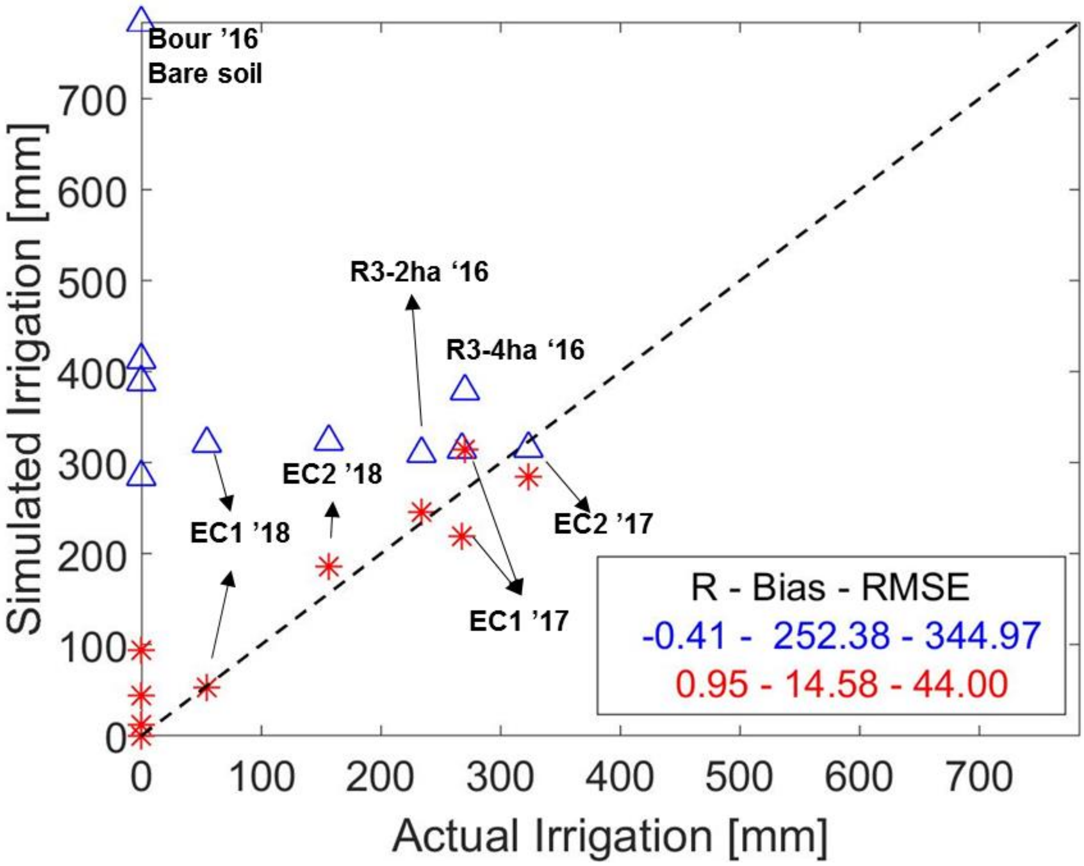

Fig. 6. Total irrigation depth applied by the farmer in the season is plotted versus the irrigation simulated by the FAO-2kc in order to avoid the water stress (blue, $I_{FAO\text{-}2Kc\_Ks=1}$) and the irrigation retrieved by the proposed approach (red, $I_{FAO\text{-}2Kc\_Landsat}$). The correlation coefficient (R), bias and root mean square error (RMSE) are shown for $I_{FAO\text{-}2Kc\_Ks=1}$ and $I_{FAO\text{-}2Kc\_Landsat}$.

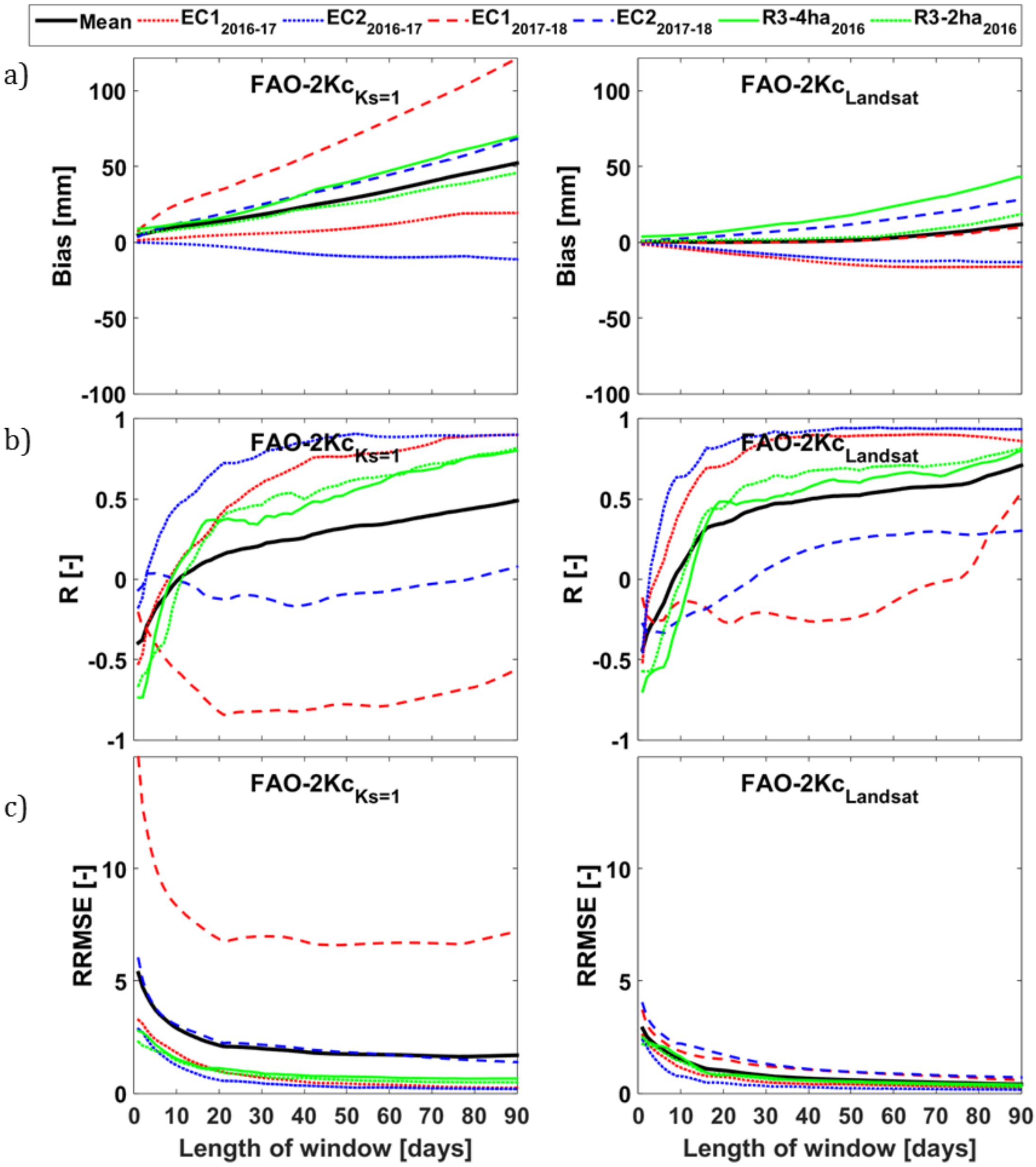

Fig. 7. Bias (a), correlation coefficient (R, b) and relative root mean square error (RRMSE, c) between observed and retrieved irrigation cumulated from 1 to 90 days through a moving window for site and season. The irrigation is retrieved by the proposed approach (FAO-2Kc$_{Landsat}$) and is also simulated by the FAO-2Kc in order to avoid water stress (FAO-2Kc$_{Ks=1}$).

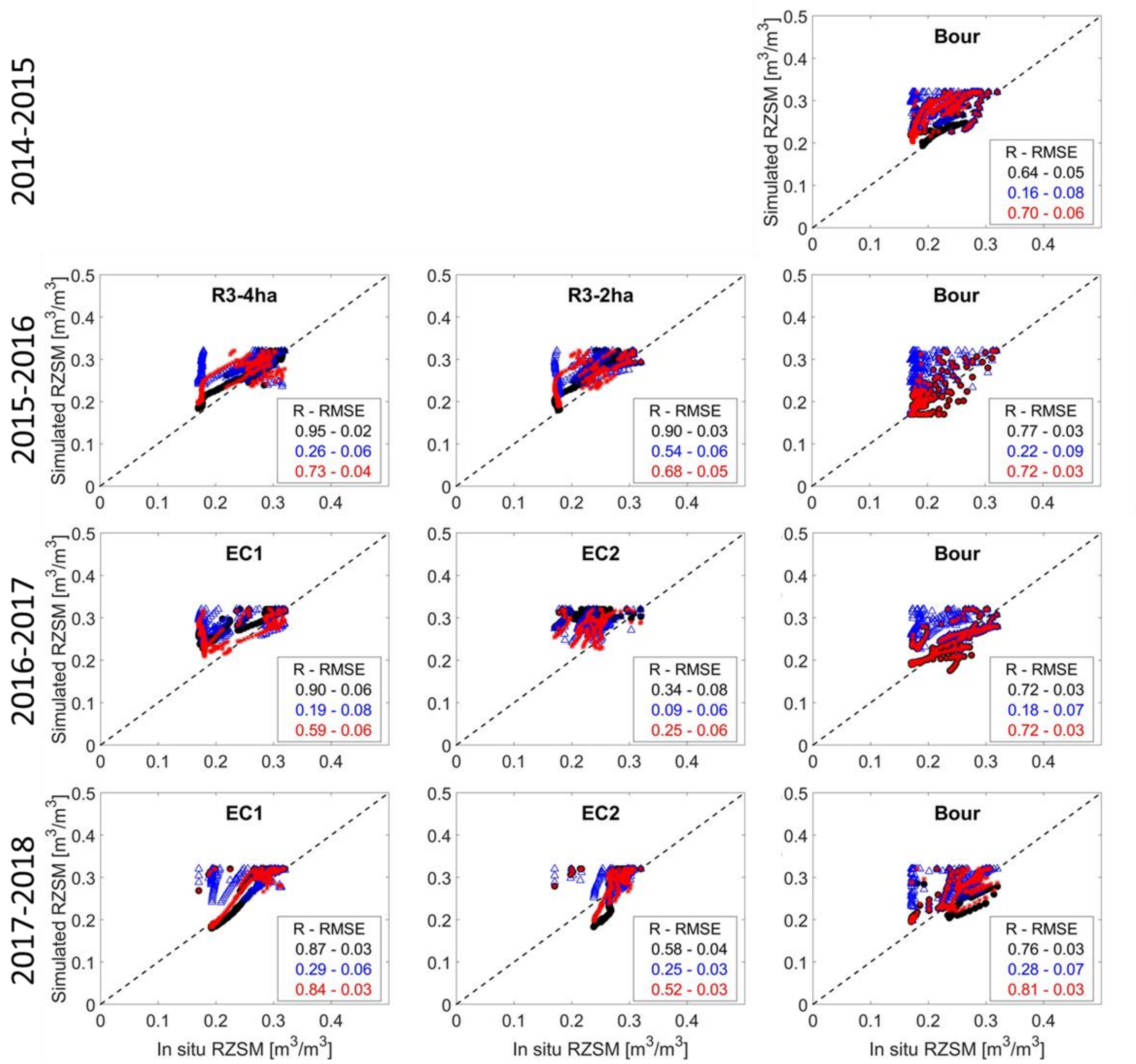

Fig. 8. Ground-based RZSM is plotted versus the RZSM simulated by the FAO-2Kc forced by observed irrigation (black), irrigation triggered by avoiding stress (blue) and irrigation retrieved from the proposed methodology (red). The correlation coefficient (R), bias and root mean square error (RMSE) are shown for RZSM from FAO-based models forced by the three different irrigation data sets.

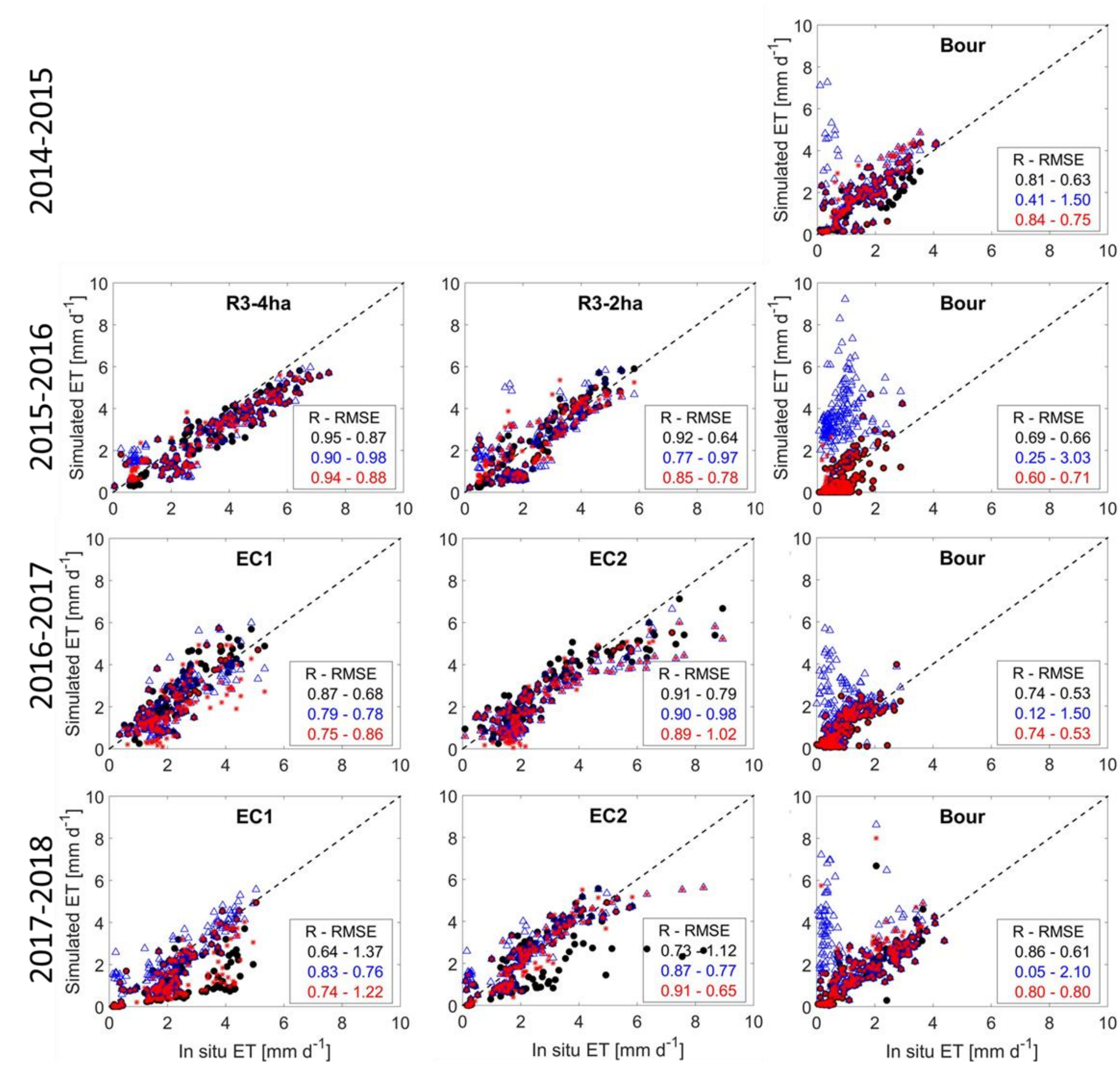

Fig. 9. Ground-based ET is plotted versus the ET simulated by from FAO-2Kc forced by observed irrigation (black, $ET_{FAO\text{-}2Kc\_Iobs}$), irrigation triggered by avoiding stress (blue, $ET_{FAO\text{-}2Kc\_Ks=1}$) and irrigation retrieved from the proposed methodology (red, $ET_{FAO\text{-}2Kc\_Landsat}$). The correlation coefficient (R), bias and root mean square error (RMSE) are shown for $ET_{FAO\text{-}2Kc\_Iobs}$, ET $ET_{FAO\text{-}2Kc\_Ks=1}$ and $ET_{FAO\text{-}2Kc\_Landsat}$.

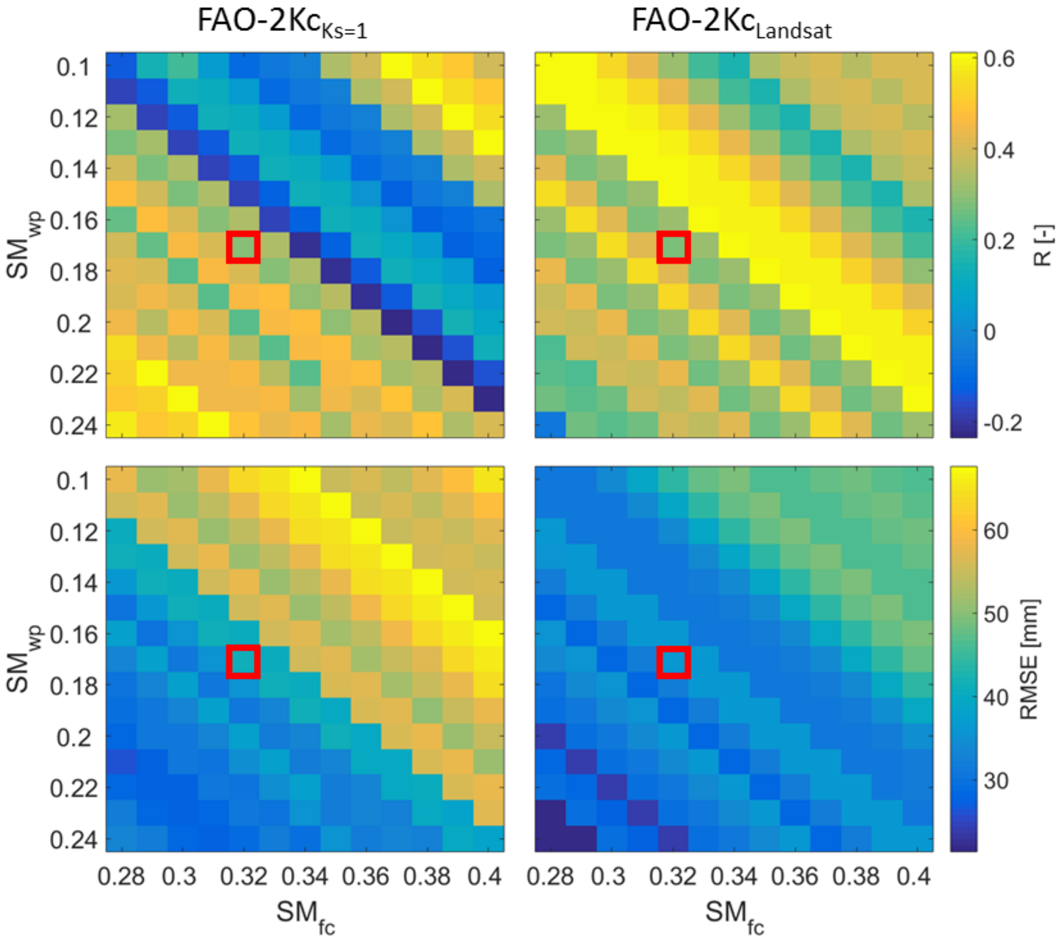

Fig. 10. Sensitivity analysis results for the soil parameters SM_{fc} and SM_{wp} by setting Zr_{max} set to 1.0 m. The irrigations are estimated by using SM_{fc} ranging between 0.28 and 0.40 m^3m^{-3} and SM_{wp} ranging between 0.10 and 0.24 m^3m^{-3}. The statistical parameter R (top) and RMSE (bottom) for actual irrigation accumulated over 15 days are estimated by using FAO-$2Kc_{Ks=1}$ (left) and FAO-$2Kc_{Landsat}$ (right) models. The red square indicates the SM_{fc} and SM_{wp} used in the approach.